

國立交通大學
光電工程研究所

碩士論文

室溫下於金屬鍍膜之氮化鎵奈米共振腔
之雷射特性

Lasing characteristics of metal-coated GaN nanocavity at room
temperature

研究生：王祐國

指導教授：郭浩中 教授

中華民國一百年六月

室溫下於金屬鍍膜之氮化鎵奈米共振腔之雷射特性

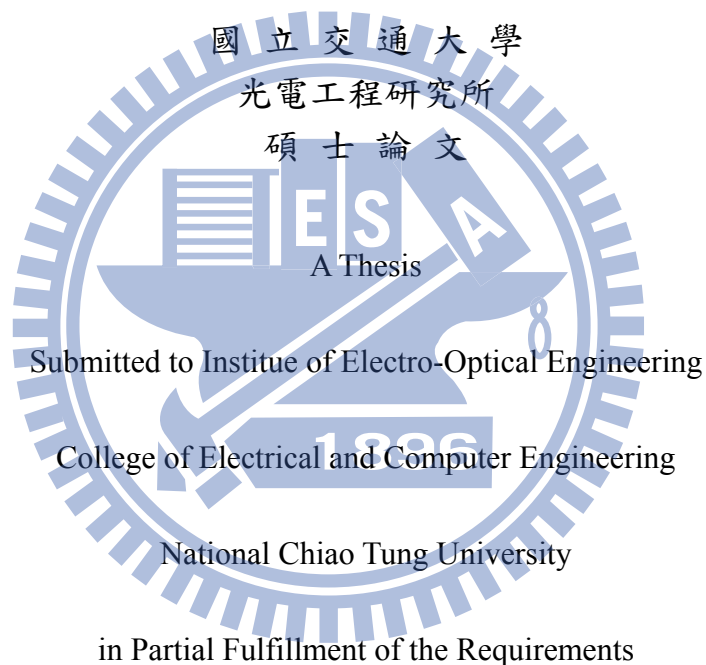
Lasing characteristics of metal-coated GaN nanocavity at room temperature

研究生：王祐國

Student：Yow-Gwo Wang

指導教授：郭浩中 教授

Advisor：Prof. Hao-Chung Kuo



for the Degree of Master

in

Electro-Optical Engineering

June 2011

Hsinchu, Taiwan, Republic of China

中華民國一百年六月

室溫下於金屬鍍膜之氮化鎵奈米共振腔之雷射特性

研究生：王祐國

指導教授：郭浩中教授

國立交通大學光電工程研究所碩士班

摘要

本論文中，我們展現了在室溫下從金屬鍍膜之氮化鎵奈米共振腔觀察到雷射訊號的可能性。

首先我們利用電子束微影在未參雜的氮化鎵薄膜上定義出條狀的結構，並在此結構上方覆蓋上一層介電質材料和鋁金屬。由微光致螢光量測系統所得的實驗結果，我們觀察到了單一模式的雷射訊號，其波長約略三百七十奈米，並由實驗結果反推出其品質因數大約為 150。除此之外，藉由模擬的方式來分析此實驗結果，我們也證明了鍍在奈米結構上的鋁金屬大大提升了此結構對於光場的局限能力。我們相信此雷射模式是由波導的模式和表面電漿的模式所混合而成的。

第二個部分，我們驗證了室溫下在金屬鍍膜之環狀奈米結構中雷射的可能性。我們利用迴音壁模式和表面電漿模式做一結合，達到在奈米結構中觀察到雷射訊號的目標。最小的環形共振腔其直徑為三微米，環的寬度約為 310 奈米。和前一章之條狀結構之元件特性做比較，我們可以得到更高的品質因子及更低的閾值能量密度，且環形的寬度更可以達到次波長的領域，並且大幅度的縮小整個元件大小。可見環形結構一如預期可利用回音壁模式來大幅提升奈米級半導體雷射的元件表現。

Lasing characteristics of meta-coated GaN nanocavity at room temperature

Student : Yow-Gwo Wang

Advisor: Prof. Hao-Chung Kuo

Institute of Electro-Optical Engineering
National Chiao Tung University

Abstract

In this thesis, we demonstrated metal-coated GaN nanocavity laser operable at room temperature by optical pumping.

We first utilized fabrication process to define the nanostripe pattern on undoped GaN layer grown on a sapphire substrate, with a thin dielectric layer and aluminum layer coated on it. From micro-photoluminescence measurement result, we observed a single mode lasing at room temperature with lasing wavelength around 370nm and the quality factor was about 150. Moreover, by simulation analysis, we proved the aluminum layer coated on the nanostripe strongly enhance the optical confinement of this nanocavity. We believed that this lasing mode was a combination of waveguide mode and surface plasmon mode.

Second, we demonstrated lasing in metal-coated GaN nanoring at room temperature. We utilize whispering-gallery-mode with surface plasmon mode to achieve lasing in a nanoring cavity. The diameter of the smallest ring is $3\mu\text{m}$, and the width of the nanoring is about 310nm. Compare with the device performance of metal-coated GaN nanostripe, we got a higher quality factor and lower threshold power density. The width of the nanoring could shrink to subwavelength scale and the size of the device can be reduced significantly. This result proved our assumption that whispering-gallery mode would improve the performance of nanolaser.

誌謝

兩年的碩士班生涯一下子就走到終點了，雖然兩年不是段很短的時間，但我依然記得剛進來時跟學長們一起學做實驗討論問題的那些時光。首先，我要感謝中研院應科中心的施閔雄老師，沒有老師的指導就不會有這本碩士論文和這些研究成果。老師的耐心指導以及所提供的意見，讓我在碩士班這段期間學到很多做研究和分析實驗的方法。這些無價之寶相信會在我未來研究之路上依舊受用無窮的。另外，我還要謝郭浩中老師的所給予的幫忙，沒有郭老師的推薦，我是沒有機會前往莊順連老師的實驗室學習的。此外，謝謝老師提供了很好的研究環境，還有平時對我的幫助與鼓勵，使我在碩士班兩年的路上能夠專注於研究上。

感謝在我初進實驗室，帶著我學習的清華學長以及 Joseph 學長，在你們的指導下我熟習到理論知識與製程技術，紮根了我對 GaN-based LED 研究的基礎，讓我可以可以學習到更多更廣的知識。再來要感謝的是振昌學長的照顧，除了一起在無塵室寫 E-beam 和做 micro-PL 的量測。學長也不厭其煩的教導我分析實驗結果和撰寫文章的技巧。另外，我還要感謝中研院應科中心的研究助理旻彥，在旻彥跟振昌學長的幫忙以及合作下，我才能有這些研究成果和發表，並且有機會可以順利完成我的碩士班學位。

此外，我要感謝李博、鏡學、閔安、智凱學長對於我在報告時提供不少想法與建議，令我收穫良多。感謝板弟、信助、Gibu、小昕、阿祥、阿菲、翁翁、哭哭、David 和小邱等學長姐，無私的和我分享實驗上的經驗與並給予我鼓勵與叮嚀，使我能有所成長。感謝羿蓁、大寶、Jolin、肉圓、祐慶、小杜、家齊、阿 po、瑋婷、Just、SGG、KAKA、冠霖、峰瑜等碩二的同學們，因為有你們使我的碩班生活增添不少快樂回憶，我會永遠記得一起做實驗討論，在無塵室打拼的時光，一起分享歡笑與宣洩壓力，很開心可以認識到可愛的大家。此外，還要感謝碩一的學弟妹們，有你們的幫忙讓我們的實驗順利許多，祝福你們明年也能順利。此外，我要感謝幫忙維護機台的各位學長跟徐先生，有你們細心照料實驗設備，讓我能順利完成實驗，做出元件。

最後要感謝我的好朋友們以及我的女朋友 Tina，感謝你們的支持，使我可以堅持下去，即使是面對低潮和困難的打擊。最後要感謝我的父母跟我的家人，你們在背後支持我、鼓勵我，並提供這麼好的環境讓我可以專心於課業上，使我能順利的取得碩士學位，謝謝你們！



Content

摘要.....	i
Abstract.....	ii
誌謝.....	iii
Content.....	v
List of Tables.....	vii
List of Figures.....	viii

Chapter 1 Introduction

1.1 History of Semiconductor Laser.....	1
1.2 GaN-based Optoelectronic Devices.....	2
1.3 Surface Plasmon Effect.....	3
1.4 Metal-coated Nano Devices.....	5
1.5 Motivation.....	6
Reference.....	12

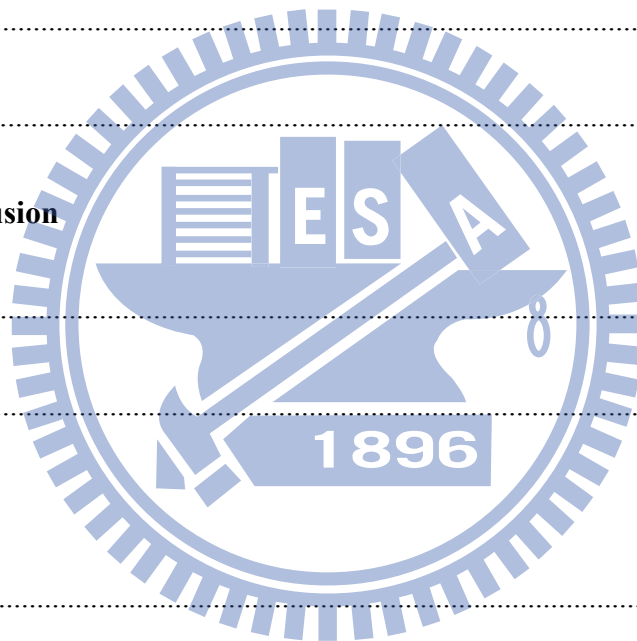
Chapter 2 Experimental Instruments and Methods

2.1 Electron Beam Lithography and Scanning Electron Microscope.....	15
2.2 Dry Etching Process and E-gun Evaporation.....	16
2.3 Micro-Photoluminescence System.....	18

Chapter 3 Lasing in Metal-coated GaN Nanostripe at Room Temperature

3.1 Epitaxial Characteristics and Fabrication Process of Metal-coated GaN Nanostripe.....	23
3.2 Lasing Characteristics of Metal-coated GaN Nanostripe.....	27
3.3 Simulation Results and Discussion.....	29

3.4 Summary.....	31
Reference.....	41
 Chapter 4 Lasing in Metal-coated GaN Nanoring at Room Temperature	
4.1 Epitaxial Characteristics and Fabrication Process of Metal-coated GaN Nanoring.....	42
4.2 Lasing Characteristics of Metal-coated GaN Nanoring.....	45
4.3 Results and Discussion.....	47
4.4 Summary.....	49
Reference.....	59
 Chapter 5 Conclusion	
5.1 Conclusion.....	60
5.2 Future Work.....	61
 Appendix	
1. Thermal Issue.....	63



List of Tables

Table 1.4 Recent Research Results on Metal-coated Nanocavity.....	11
Table 4.2 Lasing Characteristics of Different Metal-coated GaN Nanoring.....	58
Table 4.3 Comparison between Metal-coated GaN Nanostripe and Nanoring.....	58



List of Figures

Figure 1.1 Dr. Robert N. Hall with Semiconductor laser.....	8
Figure 1.2 Basic structure of GaN-based LDs and LEDs.....	8
Figure 1.3.1 Schematic representation of SPPs and its electric field distribution at the interface.....	9
Figure 1.3.2 Electric Field distribution of dielectric waveguide and plasmonic waveguide.....	9
Figure 1.3.3 Applications of surface plasmon effect: (a) Biosensor. (b) Bioimaging. (c) Lithography (d)Nanolaser.....	10
Figure 2.1.1 Schematic Diagram of E-beam Lithography System.....	18
Figure 2.1.2 JSM-6500 E-beam Lithography System.....	18
Figure 2.1.3 JSM-7000F SEM System.....	19
Figure 2.2.1 ICP-RIE System (Oxford Plasmalab System100).....	19
Figure 2.2.2 ICP-RIE System (SAMCO RIE-101PH).....	20
Figure 2.2.3 E-gun Evaporation System (ULVAC EBX-8C).....	20
Figure 2.3.1 Schematic Diagram of Micro-Photoluminescence System.....	21
Fig. 3.1.1 Process Flow Chart for Metal-coated GaN nanostripe.....	33
Fig. 3.1.2 SEM Image of Metal-coated GaN Nanostripe (a) Top View of the GaN Nanostripe before Deposition of Shielding Layers. (b) Angle View of One side of the GaN Nanostripe before Deposition of Shielding Layer.....	34

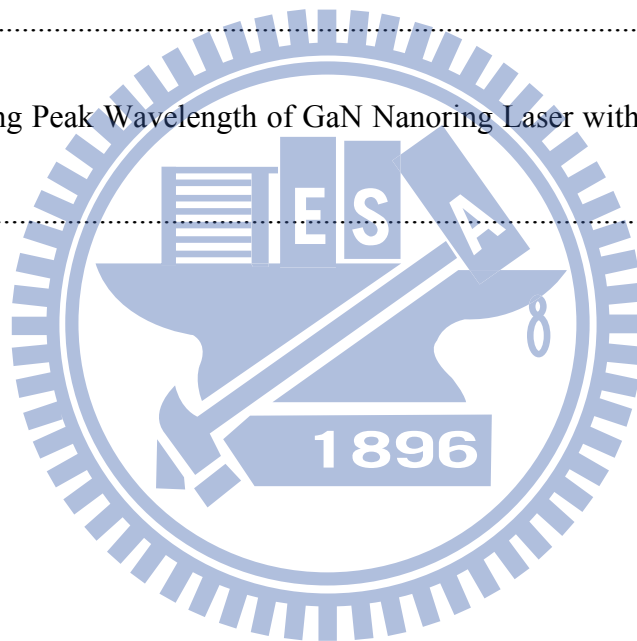
Fig. 3.1.3 Angle View of the GaN Nanostripe after the Deposition of SiO ₂ and Aluminum Layers.....	35
Fig. 3.1.4 Schematic Diagram of Metal-coated GaN Nanostripe.....	35
Fig. 3.2.1 PL Spectrum of Undoped GaN Layer with and without Metal and Dielectric Shielding Layers.....	36
Fig. 3.2.2 PL Spectrum of Metal-coated GaN Nanostripe Above (Red) and Below (Black) Threshold.....	36
Fig. 3.2.3 Light-in and Light-out Curve and the Linewidth of Lasing Peak.....	37
Fig.3.3.1 (a) The E _z Mode Profile of the Nanostripe without Shielding Layers. (b) The E _z Mode Profile of the Nanostripe with Shielding Layers.....	38
Fig. 3.3.2 Schematic Diagram of the Nanostripe Model in Effective Index Method.....	39
Fig. 3.3.3 Effective Structure of Nanostripe under TE Mode.....	39
Fig. 3.3.4 TE Mode Band Diagram of Nanostripe.....	40
Fig. 4.1.1 Process Flow Chart for Metal-coated GaN Nanostripe.....	51
Fig. 4.1.2 SEM Image of different size of GaN Nanoring before shielding layer deposition (a) 7μm in diameter. (b) 5μm in diameter. (c) 3μm in diameter.....	52
Fig.4.1.4Schematic Diagram of Metal-coated GaN Nanostripe.....	53
Fig. 4.2.1 Lasing Characteristics of Metal-coated GaN Nanoring with 7μm in diameter (a) Spectrum Above (Red) and Below (Black) Threshold. (b)L-L Curve and the Linewidth of the	

Lasing Peak.....54

Fig. 4.2.2 Lasing Characteristics of Metal-coated GaN Nanoring with 5 μ m in diameter (a) Spectrum Above (Red) and Below (Black) Threshold. (b)L-L Curve and the Linewidth of the Lasing Peak.....55

Fig. 4.2.3 Lasing Characteristics of Metal-coated GaN Nanoring with 3 μ m in diameter (a) Spectrum Above (Red) and Below (Black) Threshold. (b)L-L Curve and the Linewidth of the Lasing Peak.....56

Fig. A.1 The Lasing Peak Wavelength of GaN Nanoring Laser with (Red) or without (Black) Metal.....64



Chapter 1 Introduction

1.1 History of Semiconductor Laser

Robert N. Hall, a researcher worked for General Electric, invented first semiconductor laser in 1962. Since then, the development of semiconductor laser had a huge progress thanks to scientists and engineers around the globe. At 1962, Nick Holonyak Jr. demonstrated first visible wavelength semiconductor laser at red wavelength region. Other groups in the world also contributed to the invention of semiconductor laser in different ways.

Since invention of semiconductor laser, it promises a huge potential for its application in the very near future. It generally becomes one of the most important types of laser in the world. It was first used for optical communication in fiber. Then with the utilization of different materials to fabricate the Laser Diodes (LDs), now we could see semiconductor lasers in our daily life like optical storage, or used in a micro projector for display, even for military purposes. Its low cost and mass-production ability make it suitable for marketing than other types of laser.

The first laser diode was made by gallium arsenide (GaAs), which emits light from optical communication to red wavelength region. Other types of material including gallium nitride (GaN) also adopted to make a laser diode with a lasing wavelength from visible to shorter wavelength region. Nowadays common lasing wavelength for laser diode is ranging from 375nm to almost 3 μm , and still under development.

1.2 GaN-based Optoelectronic Devices

Gallium nitride (GaN) is a compound semiconductor with direct bandgap, which is a crucial characteristic for radiative recombination. It is a wide band gap (3.4 eV) material which makes it a suitable candidate for the application of optoelectronic devices, including GaN-based Light Emitting Diodes (LEDs) and LDs operating in blue or ultra-violet (UV) wavelength regions and other devices.

GaN-based LEDs fill the void on the primary color, and make white light LEDs possible with the combination of phosphor or LED with different colors. Thanks to intensive development in recent years [1-4], the manipulation of GaN material system has been mature enough to create high-brightness GaN LEDs in blue wavelength. This progress makes LEDs possible for the applications in display or solid-state lighting, and might one day replace the light bulb which used by human beings for many years.

At the same time, GaN-based semiconductor lasers' lasing wavelength in blue or UV wavelength region has also developed by scientist. Since the demonstration by Nakamura *et al.* [5] the first GaN-based laser lasing operated under room temperature continuous-wave (CW) condition at 1996, many applications of GaN-based have been achieved in recent years. Its application like blue-ray disks or as a light source in a micro-projector already exists in our daily life. Fig. 1.2 shows typical structures of GaN-based LDs and LEDs.

Moreover, GaN-based vertical-cavity surface emitting laser (VCSEL) has been

developed for many years [6-9]. At 2008, T. C. Lu *et al.* developed GaN-based VCSELS operated under continuous wave condition at room temperature [7]. It has some advantages like single-longitudinal-mode operation, symmetric and low divergence angle, and two dimensional array capabilities makes VCSELS very competitive compared with edge emitting laser. These merits make GaN-based VCSELS have many applications in our daily life.

1.3 Surface Plasmon Effect

Surface plasmon polaritons (SPPs) are light waves trapped on the surface because of electron gas couple with photons. It is a kind of electromagnetic wave propagating on the interface between two materials which change sign on their real part of dielectric constant. For example: a metal-dielectric interface. The SPPs existed at the interface between dielectric materials and metal could attribute to resonant coupling of photons from the polarized light with the oscillation of metal free electron. Fig. 1.3.1 shows the schematic representation of an electron density wave propagating along a metal-dielectric interface and the electric field distribution around the interface.

SPPs could concentrate and channel light under subwavelength scale, which has a huge potential on exploring science phenomenon under such small scale, and this might one day help scientists and engineers to make photonic integrated circuit with a smaller size than we have now. This kind of structure also solves the problem that dielectric waveguide would show poor confinement under subwavelength region. Fig. 1.3.2 shows the distribution of

optical field for these two waveguide structures. The other advantage is surface plasmon effect concentrates light in this way leads to an electric field enhancement that can be used to manipulate light-matter interactions and boost non-linear phenomena. Therefore, lots of applications have been developed for many years and exist in our daily life [10-13]. For example, bioimage , biosensor , advanced lithography technique, and nanolaser.

It is the most difficult task for researchers to observe the behavior of a bio molecule. Therefore, in order to observe this tiny molecule with the size in just a few nanometers, researchers utilize surface plasmon effect to improve the extraction of light. With this new technique, researchers could observe their samples and distinguish its details even in subwavelength region. For biosensor, the utilization of surface plasmon effect makes the test sample become label free and can be detected directly in real time. This has been applied to drug screening, kinase analysis and research on antibody development [10]. To further lower the cost of production for a single chip, a better lithography is needed to put more patterns on a single wafer, the e-beam lithography and other techniques are still struggling on their throughput, which is too low to become commercialize. A set of plasmonic mirrors takes the advantages of surface plasmon effect and demonstrate lithography technique with a linewidth only 80nm recently [11]. This new method has showed a promising way to the development of nanolithography. Moreover, taking the advantages of energy confinement and field enhancement, researchers have achieved making a semiconductor laser in subwavelength

scale even with the lossy metal coated on it [13]. Many research teams have reported their result using different metals and cavity. This will discuss thoroughly in the following section.

Fig. 1.3.3 shows some examples of the application of surface plasmon effect.

1.4 Metal-coated Nano Devices

Metal-coated cavity has been intensely researched by scientist around the world. It could reduce the size of a semiconductor laser to nano scale, even in subwavelength scale. This result breaks the diffraction limit which constrains the size of a laser that cannot be smaller than its nature wavelength. The lasing characteristics also be studied by researchers trying to explain the physical meaning behind the experimental result.

At 2007, Martin T. Hill *et al.* demonstrated lasing in metal-coated nanocavity [13]. They coated silver and dielectric layer on the nanorod and observe lasing signal at 77 K. After that, different designs of metal-coated nanocavity have reported experimentally or theoretically.

Metal-coated waveguide structure had also been demonstrated by the same research team and bow-tie nanostructure had been proposed by S. W. Chang *et al.* [14]. The combination of surface plasmon effect and bow-tie structure shows a promising way theoretically in forming a semiconductor laser. Moreover, different kinds of metal have been use to form metal-coated nanocavity. From recent research results [13-17], people use silver, gold and aluminum to form the nano structure. At 2010, M. P. Nezhad *et al.* [15] demonstrated a metal-coated nanocavity

with aluminum layer and SiO₂ as the dielectric layer. They also proposed a theoretical analysis to show that optimization of the dielectric layer could have a higher chance to get a better quality factor to achieve lasing action. K. Y. Yu *et al.* at 2010 demonstrated a nano-patch laser with metal coated above and below the gain medium, and analyze the lasing characteristics of the device [16]. In 2011, M. W. Kim *et al.* demonstrated lasing in a metal-clad microring [17]. In conclusion, metal-coated nanocavity has been demonstrated experimentally in different structures includes nanorod, waveguide, and ring. In sum, recent research results mainly focus on InGaAsP material system, which has a lasing wavelength from red to Infar-red region. Table 1.4 shows some important research results did by researchers around the world in recent years.

1.5 Motivation

Metal-coated nanocavity shows huge potential to reduce the size of semiconductor laser into subwavelength scale. However, their research results mainly focus on InGaAsP material system and optical communication to infra-red wavelength region. Shorter lasing wavelength and other material systems have not yet been reported by any groups in the world.

In this thesis, we utilize GaN as the gain medium for metal-coated nanocavity, combining with aluminum and SiO₂ layer. We use E-beam lithography to define two different types of nano structure, and then we use dry etching processes and other fabrication process to form the metal-coated GaN nanocavity. We analyze the lasing characteristics of our metal-coated nano

devices which is optical pumped under room temperature pulsed condition, then we use finite element method and effective index method to further simulate our structure and discuss the physics behind the experiment result.

In chapter 2, we briefly introduce the instruments which are used to fabricate the device and measure its characteristics. Then in chapter 3, we present experiment and simulation result of lasing in a metal-coated GaN nanostripe at room temperature. The waveguide structure is only 500nm in its width. In chapter 4, we use E-beam lithography to define a nanoring pattern on the undoped GaN layer. We also perform measurement on different sizes of nanoring laser range from $7\mu\text{m}$ to $3\mu\text{m}$, coated with the aluminum layer. By the combination of nanoring structure and the advantages of metal-coated nanocavity, we could shrink the size of our nanostructure into smaller scale and better device performance. Finally in chapter 5, we will give a brief conclusion of this thesis.

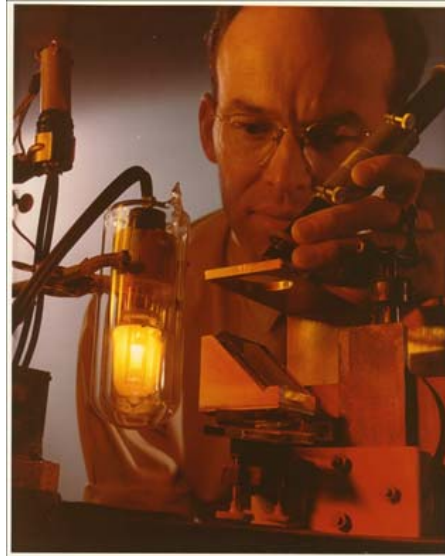


Fig. 1.1 Dr. Robert N. Hall with Semiconductor Laser.

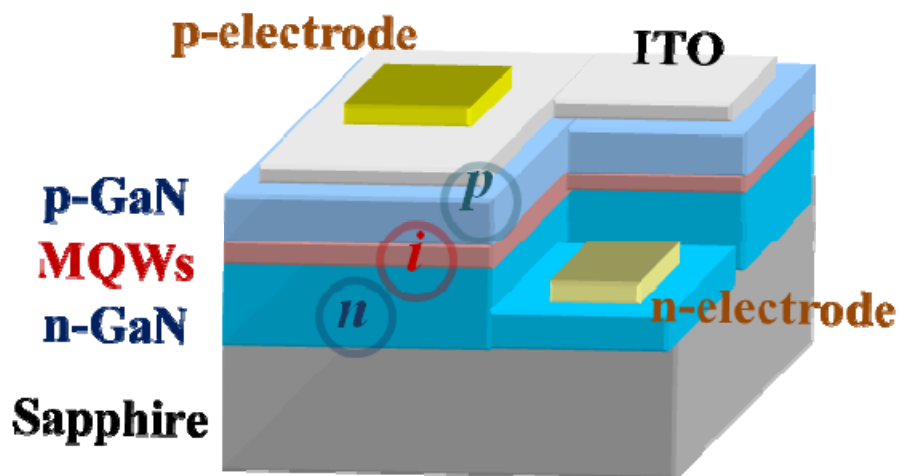
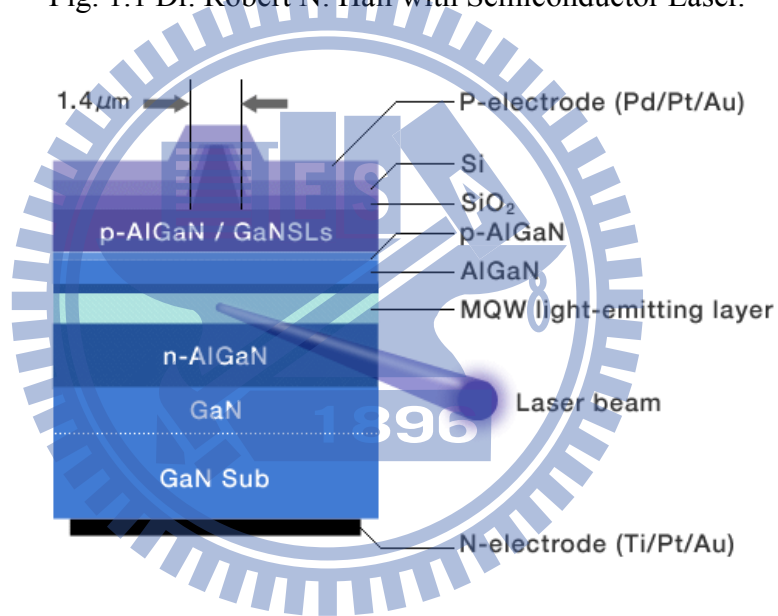


Fig. 1.2 Basic structure of GaN-based LDs and LEDs.

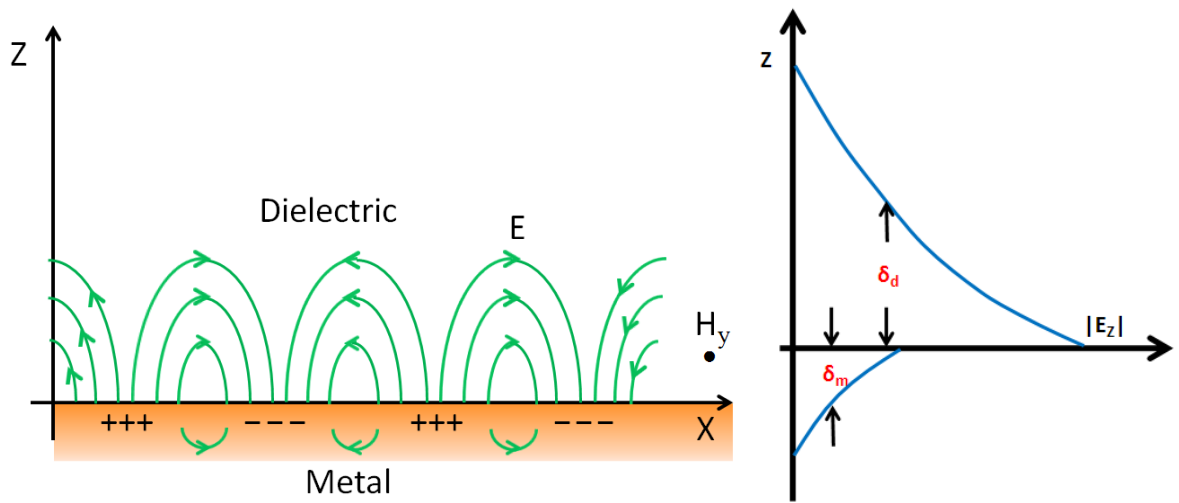


Fig. 1.3.1 Schematic representation of SPPs and its electric field distribution at the interface.

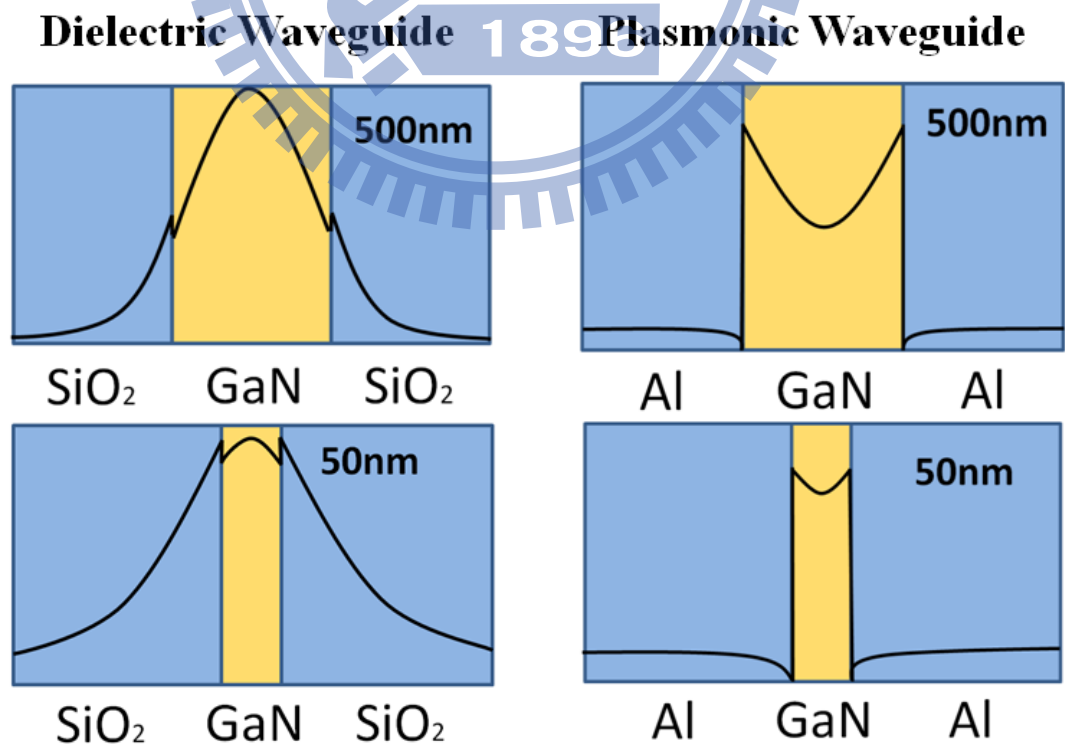


Fig. 1.3.2 Electric Field distribution of dielectric waveguide and plasmonic waveguide.

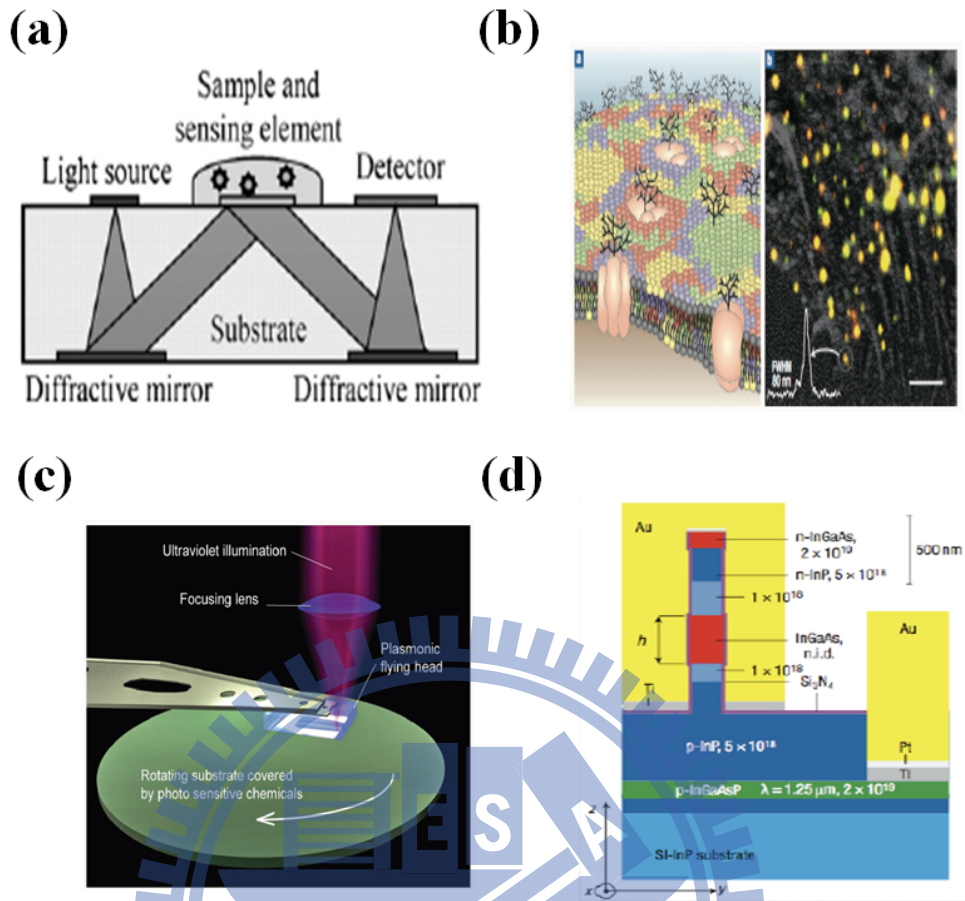
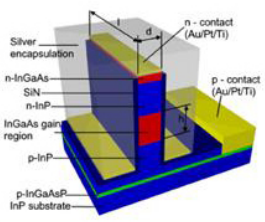
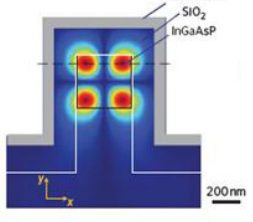
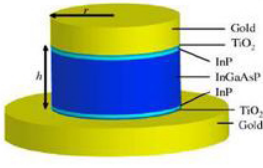
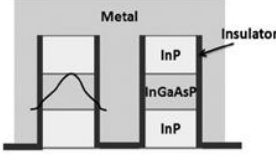
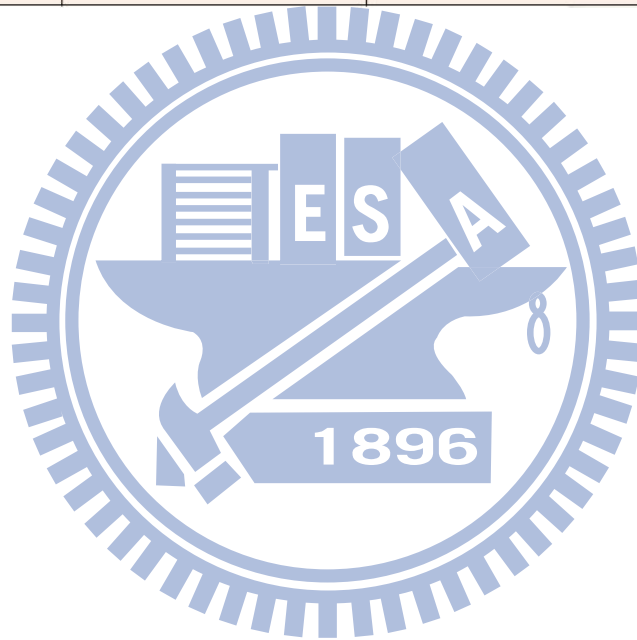


Fig. 1.3.3 Applications of surface plasmon effect: (a) Biosensor. (b) Bioimaging. (c) Lithography (d) nanolaser.

Table 1.4 Recent Research Results on Metal-coated Nanocavity.

			
<p>M. T. Hill et al. InGaAs $\lambda: \sim 1.5 \mu\text{m}$ (2009)</p>	<p>M. P. Nezhad et al. InGaAsP $\lambda: 1.43 \mu\text{m}$ (2010)</p>	<p>K. Yu et al. InGaAsP $\lambda: \sim 1.4 (\mu\text{m})$ (2010)</p>	<p>M. W. Kim et al. InGaAsP $\lambda: \sim 1.35 (\mu\text{m})$ (2011)</p>
<p>TUE</p>	<p>UCSD</p>	<p>UCB</p>	<p>UMich</p>



References

- [1] S. Nakamura, M. Senoh, N. Iwasa, and S. Nagahama, "High brightness InGaN blue, green, and yellow light-emitting diodes with quantum structures," *Jpn. J. Appl. Phys.*, vol. **34**, pp. L797, 1995.
- [2] M. H. Kim, M. F. Schubert, Q. Dai, J. K. Kim, and E. F. Schubert, J. Piprek, and Y. Park, "Origin of efficiency droop in GaN-based light-emitting diodes," *Appl. Phys. Lett.*, vol. **91**, pp. 183507, 2007.
- [3] C. H. Wang, S. P. Chang, W. T. Chang, J. C. Li, Y. S. Lu, Z. Y. Li, H. C. Yang, H. C. Kuo, T. C. Lu, and S. C. Wang, "Efficiency droop alleviation in InGaN/GaN light-emitting diodes by graded-thickness multiple quantum wells," *Appl. Phys. Lett.*, vol. **97**, pp. 181101, 2010.
- [4] S. D. Lester, F. A. Ponce, M. G. Craford, and D. A. Steigerwald, "High dislocation densities in high efficiency GaN-based light-emitting diodes," *Appl. Phys. Lett.*, vol. **66**, pp. 1249, 1995.
- [5] S. Nakamura, M. Senoh, S. I. Nagahama, N. Iwasa, T. Yamada, T. Matsushita, Y. Sugimoto, and H. Kiyoku, "Room-temperature continuous-wave operation of InGaN multi-quantum-well structure laser diodes," *Appl. Phys. Lett.*, vol. **69**, pp. 4056, 1996.
- [6] J. T. Chu, T. C. Lu, H. H. Yao, C. C. Kao, W. D. Liang, J. Y. Tsai, H. C. Kuo, and S. C. Wang, "Room-temperature operation of optically pumped blue-violet GaN-based vertical-cavity surface-emitting lasers fabricated by laser lift-off," *Jpn. J. Appl. Phys.*, vol. **45**,

pp. 2556, 2006.

[7] T. C. Lu, C. C. Kao, H. C. Kuo, G. S. Huang, and S. C. Wang, "CW lasing of current injection blue GaN-based vertical cavity surface emitting laser," *Appl. Phys. Lett.*, vol. **92**, pp. 141102, 2008.

[8] C. C. Kao, T. C. Lu, H. W. Huang, J. T. Chu, Y. C. Peng, H. H. Yao, J. Y. Tsai, T. T. Kao, H. C. Kuo, S. C. Wang, and C. F. Lin, "The lasing characteristics of GaN-based vertical-cavity surface-emitting laser with AlN/GaN and Ta₂O₅/SiO₂ distributed bragg reflectors," *IEEE Photonic Tech. Lett.*, vol. **18**, pp. 877, 2006.

[9] T. C. Lu, S. W. Chen, T. T. Wu, P. M. Tu, C. K. Chen, C. H. Chen, Z. Y. Li, H. C. Kuo, and S. C. Wang, "Continuous wave operation of current injection GaN vertical-cavity surface emitting laser at room temperature," *Appl. Phys. Lett.*, vol. **97**, pp. 071114, 2010.

[10] X. D. Hoa, A. G. Kirk, M. Tabrizian, "Towards integrated and sensitive surface plasmon resonance biosensors: A review of recent progress," *Biosensors and Bioelectronics*, vol. **23**, pp. 151, 2007.

[11] W. Srituravanich, L. Pan, Y. Wang, C. Sun, D. B. Bogy, and X. Zhang, "Flying plasmonic lens in the near field for high-speed nanolithography," *Nat. Nanotechnology* vol. **3**, pp. 733, 2008.

[12] M. F. Garcia-Parajo, "Optical antennas focus in on biology," *Nat. Photonics*, vol. **2**, pp. 201, 2008.

[13]M. T. Hill, Y. S. Oei, B. Smallbrugge, Y. Zhu, T. de Vries, P. J. van Veldhoven, F. W. M. van Otten, T. J. Eljkemans, J. P. Turkiewicz, H. de Waardt, E. J. Geluk, S. H. Kwon, Y. H. Lee, R. Notzel, and M. K. Smit, "Lasing in metallic-coated nanocavities," Nat. Photonics, vol. **1**, pp. 589, 2007.

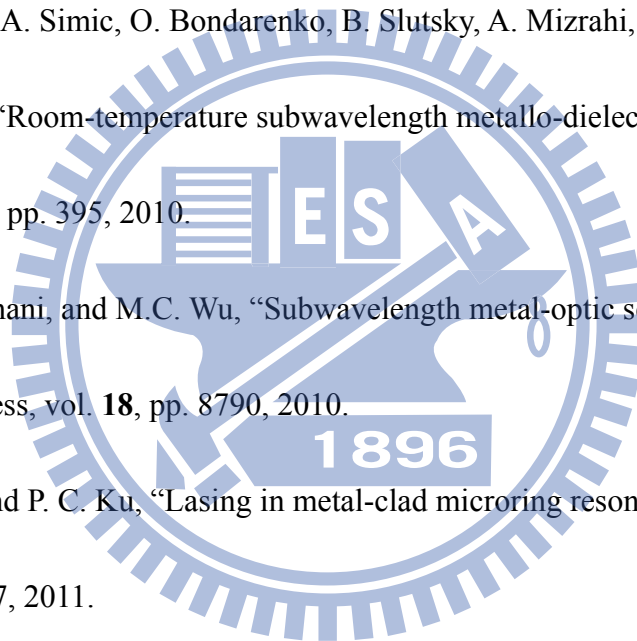
[14]S. W. Chang, C. Y. A. Ni, S. L. Chuang, "Theory for bowtie plasmonic nanolasers," Opt. Express, vol. **16**, pp. 10580, 2008.

[15]M. P. Nezhad, A. Simic, O. Bondarenko, B. Slutsky, A. Mizrahi, L. Feng, V. Lomakin, and Y. Fainman, "Room-temperature subwavelength metallo-dielectric lasers," Nat. Photonics, vol. **4**, pp. 395, 2010.

[16]K. Yu, A. Lakhani, and M.C. Wu, "Subwavelength metal-optic semiconductor nanopatch lasers," Opt. Express, vol. **18**, pp. 8790, 2010.

[17]M. W. Kim, and P. C. Ku, "Lasing in metal-clad microring resonator," Appl. Phys. Lett., vol. **98**, pp. 131107, 2011.

http://www.sony.net/SonyInfo/technology/technology/theme/laser_diode_01.html



Chapter 2 Experimental Instruments and Methods

2.1 Electron Beam Lithography and Scanning Electron Microscope (SEM)

Electron Beam Lithography System

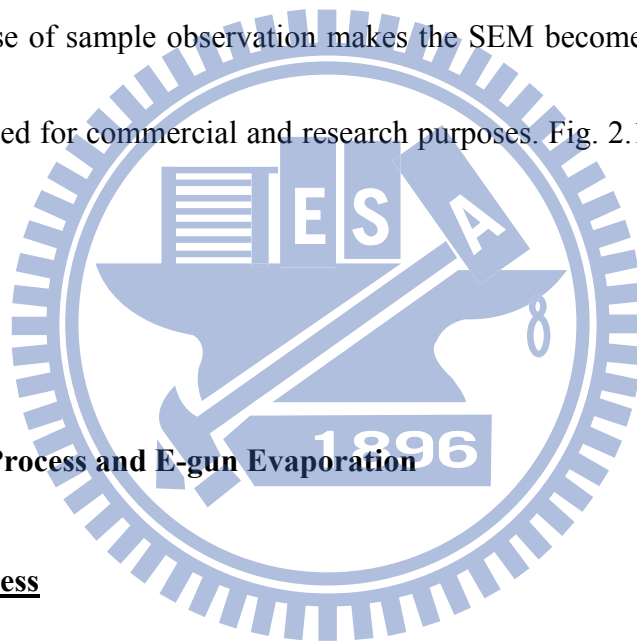
Electron beam lithography, usually call as E-beam lithography, is a technique to utilize a beam of electrons to exposing the photo resist on the surface of a material, then selectively removing the photo resist on the film to transfer the pattern we want onto the film. This could break the diffraction limit which constrains conventional photo lithography technique, and shows a promising chance to fabricate device in nano-scale.

The E-beam lithography system usually consists of an electron gun as source of electron, lenses for focusing, stage for moving the sample precisely under the electron beam, a beam blanker to control the exposure time of electron beam and a computer to control the whole system and the pattern. Fig. 2.1.1 shows the schematic diagram.

For most of E-beam lithography system used for commercial applications are very expensive; therefore, for academic purpose, people usually convert an electron microscope into an E-beam lithography system with a relatively low cost. For thesis, we use an E-beam lithography system converted from a scanning electron microscope using JSM-6500 made by JEOL as shown in Fig. 2.1.2.

Scanning Electron Microscope

Scanning electron microscope (SEM) is one of the most important equipment for people to observe objects in nano-scale. The electrons interact with atoms that make up the sample producing signals that contain information's about itself. Moreover, preparation of the samples for SEM is relatively easy due to the fact that SEM only require the sample to be conductivity. The combination of higher magnification, larger depth of focus, greater resolution, and ease of sample observation makes the SEM becomes one of the most widely used equipment used for commercial and research purposes. Fig. 2.1.3 shows the JSM-7000F made by JEOL.



2.2 Dry Etching Process and E-gun Evaporation

Dry Etching Process

Dry etching process is critical for scientists to fabricate the device according to their plan, and there are two types of etching processes: wet etching and dry etching. Dry etching process uses plasma to etch the semiconductor material and it is a kind of anisotropic etching process. The linewidth of dry etching process is smaller than wet etching, therefore, dry etching process gradually replace wet etching process after 1980.

The mechanism of dry etching process is as follow: first, the etching gas has been

diffuse to chamber under ultra-low pressure. Second, when the pressure is stable, plasma is produced by RF frequency. Third, the radicals produced by bombardment of high speed electron would diffuse to the wafer and attach to its surface. Fourth, with the help of ion bombardment, these radicals would react with the atoms on the surface and form by-product as gas. At the end, these volatile by-products would then leave the surface of wafer and discharge from chamber. Fig. 2.2.1 shows the inductively coupled plasma and reactive ion etching (ICP-RIE) system used to etch Si_3N_4 layer to transfer the patten from PMMA layer, and Fig. 2.2.2 shows the ICP-RIE equipment used to etch GaN layer.

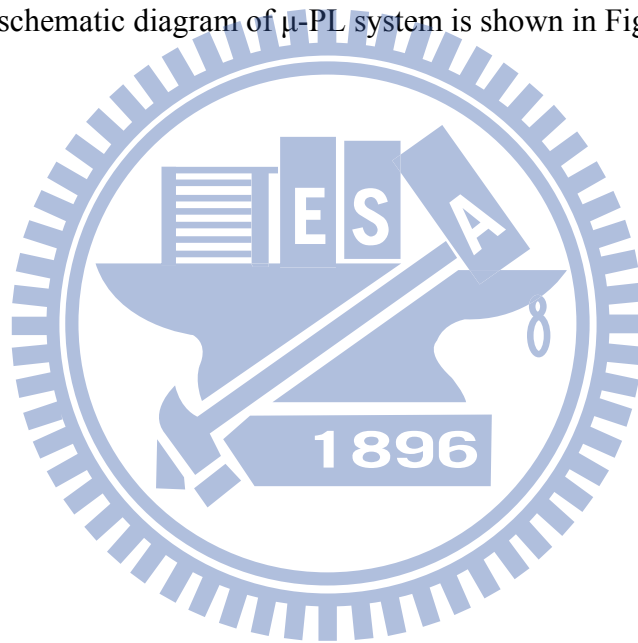
E-gun Evaporation

E-gun evaporation, also called as E-beam evaporation, is one kind of physical vapor deposition (PVD). The difference of E-gun evaporation is that it uses electron beam to heat up the source material. The advantage of E-gun evaporation is that it could heat only one small part of the surface of the source material. This will reduce the energy consumption used by PVD. Therefore, it is a common way to use E-gun evaporation to deposit metal on to the device.

For an E-gun evaporation system, it consists of an electron beam evaporation gun, a system controller, power supply, evaporation material, its crucibles, and sample to be coated. All the processes are conducted under very low pressure, in a vacuum chamber. Fig. 2.2.3 shows the E-gun evaporation system.

2.3 Micro-Photoluminescence (μ -PL) System

Micro-Photoluminescence is an advanced Photoluminescence system to measure sample in micrometer even nanometer scale. The spot size of the light source for μ -PL system has shrunk to micrometer scale to observe the optical properties of sample. In our μ -PL system, we use Nd:YVO₄ laser with lasing wavelength 355nm as a pumping source, and the spot size is about 50 μ m, frequency of the laser is 1 kHz, and the pulse width is about 500 ps. The schematic diagram of μ -PL system is shown in Fig. 2.3.1.



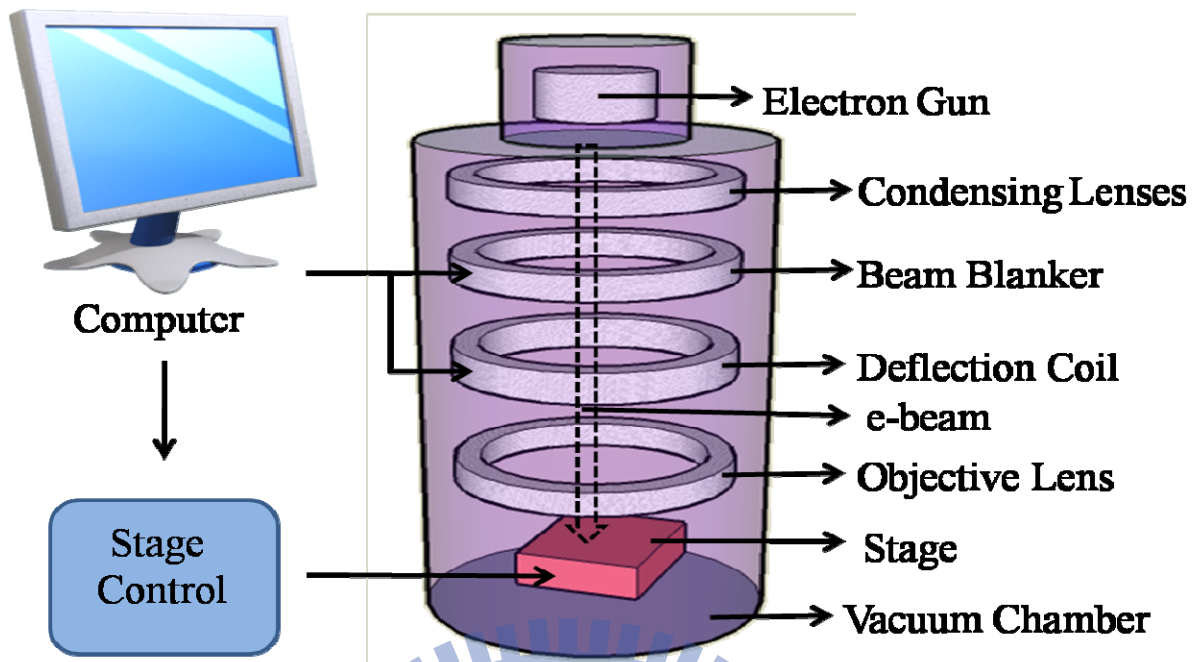


Fig. 2.1.1 Schematic Diagram of E-beam Lithography System.



Fig. 2.1.2 JSM-6500 E-beam Lithography System.



Fig. 2.1.3 JSM-7000F SEM System.



Fig. 2.2.1 ICP-RIE System (Oxford Plasmalab System 100).



Fig. 2.2.2 ICP-RIE System (SAMCO RIE-101PH).

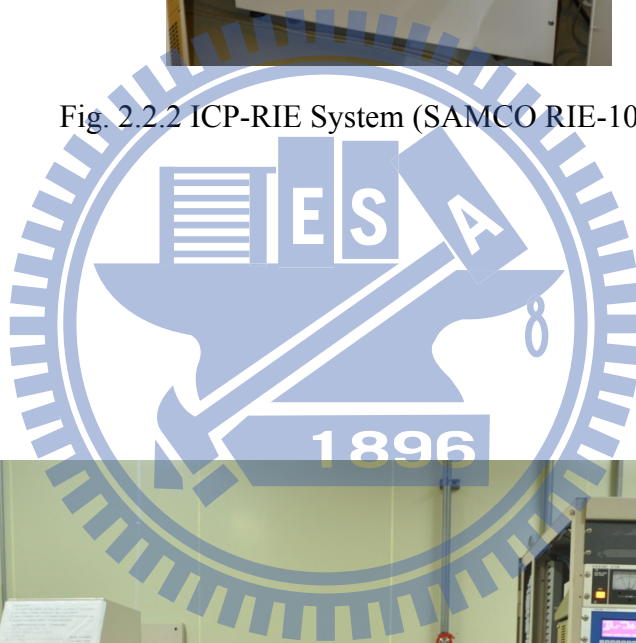


Fig. 2.2.3 E-gun Evaporation System (ULVAC EBX-8C).

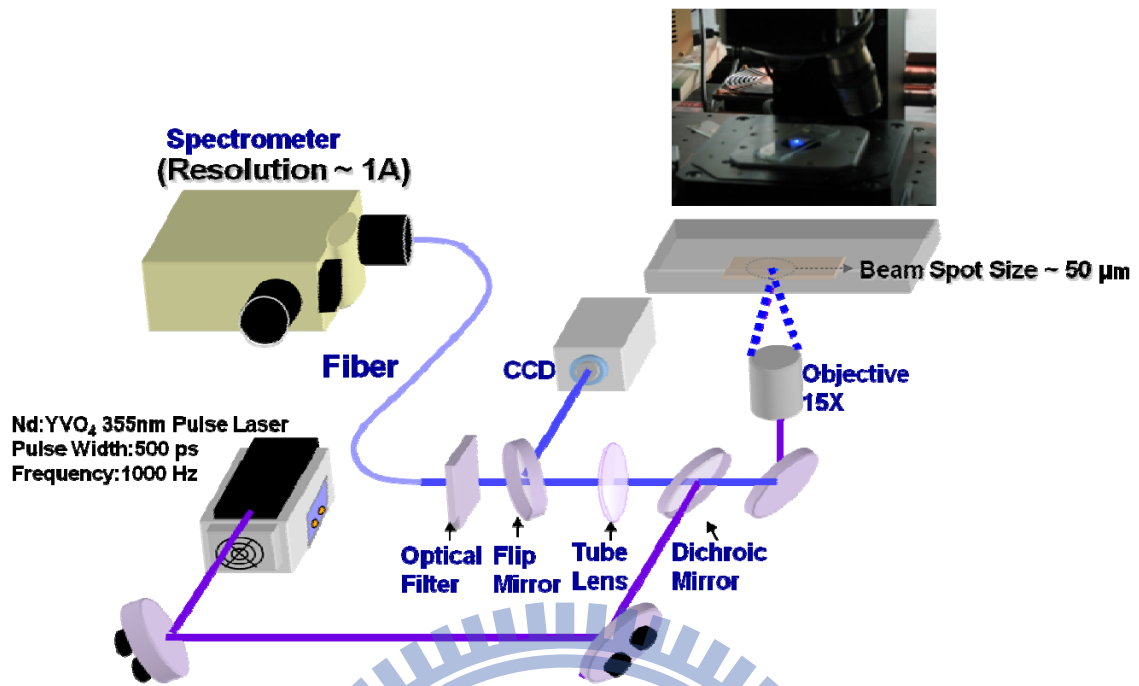
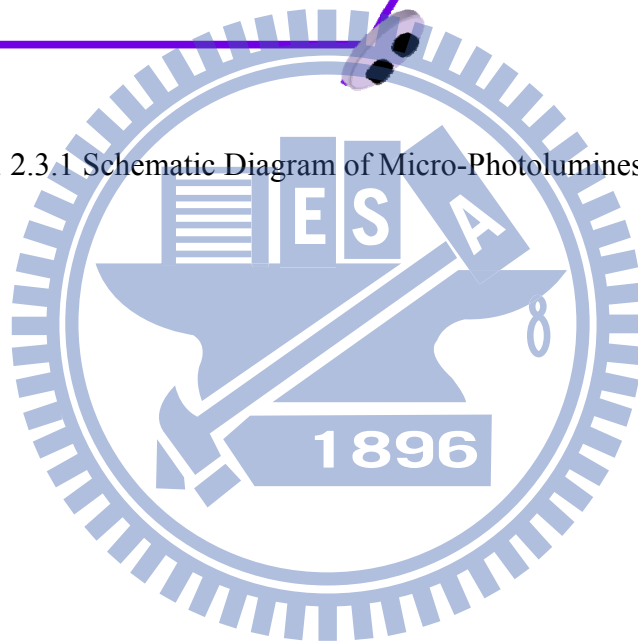


Fig. 2.3.1 Schematic Diagram of Micro-Photoluminescence System.



Chapter 3 Lasing in Metal-coated GaN Nanostripe at Room Temperature

3.1 Epitaxial Characteristics and Fabrication Process of Metal-coated GaN Nanostripe

We use undoped GaN layer grown on C-plane (0001) sapphire substrate as gain medium. The thickness of the undoped GaN layer is about 2 μ m. Metal-organic chemical vapor deposition (MOCVD) system (EMCORE D-75) is used to grow undoped GaN layer on the polished optical-grade C-plane (0001), 2 inches sapphire substrate. Trimethylgallium (TMGa) and Ammonia (NH₃) were used as the Ga and N sources respectively.

First, a thermal cleaning process was carried out at 1080°C for 10 minutes in a stream of hydrogen ambient before the growth of epitaxial layers to clean the sample surface. Second, the 30nm thick GaN nucleation layer was first grown on the sapphire substrate at 530°C, and at the end the 2 μ m thick undoped GaN layer was grown on it at 1040°C.

After we finish the preparation of sample, we adopt some fabrication processes to complete our device. The complete process flow chart for our device is shown in Fig. 3.1.1.

First, we deposit 300nm thick Si₃N₄ layer on the undoped GaN layer as an etching mask for the following E-beam lithography process. Second, for E-beam lithography process, we use spin coater to put a thin polymethylmethacrylate (PMMA) on the sample, then the nanostripe pattern was defined using E-beam lithography system. After this, we use ICP-RIE dry etching system to transfer the pattern on the PMMA layer onto the Si₃N₄. And then transfer the pattern again onto the undoped GaN layer to form the nanostripe structure on it. Fig.

3.1.2 shows the SEM image of nanostripe from top view and angled view after these processes.

Third, before we start to do the next step, we use wet etching methods to clean our sample, washing away the particles created in the previous dry etching processes to promote the performance of our device. After this, we use plasma enhanced chemical vapor deposition (PECVD) to deposit a thin SiO₂ layer on the GaN nanostripe for just 20nm. At the end, we use E-gun evaporation to deposit a 60nm thick aluminum layer to complete our device. The SEM image of our device after the deposition of dielectric layer and metal is shown in Fig. 3.1.3 in angled view. The detail recipe of each process is shown in the following paragraphs, and the schematic diagram of metal-coated GaN nanostripe is shown in Fig. 3.1.4.

PECVD (SAMCO PD220)

- Si₃N₄ film deposition:

SiH₄/Ar: 20sccm

NH₃:10sccm

N₂:490sccm

Temperature: 300°C

RF Power: 35W

Pressure: 100Pa

Time: 31min. for 300nm thick Si₃N₄

- SiO₂ film deposition:

SiH₄/Ar: 25sccm

N₂O:500sccm

N₂:250sccm

Temperature: 250°C

RF Power: 35W

Pressure: 120Pa

Time: 1min. for 20nm thick SiO₂

ICP-RIE (Oxford Plasmalab System 100)

- Si₃N₄ film etching:

Ar/O₂: 5sccm

CHF₃: 50sccm

RF Power: 150W

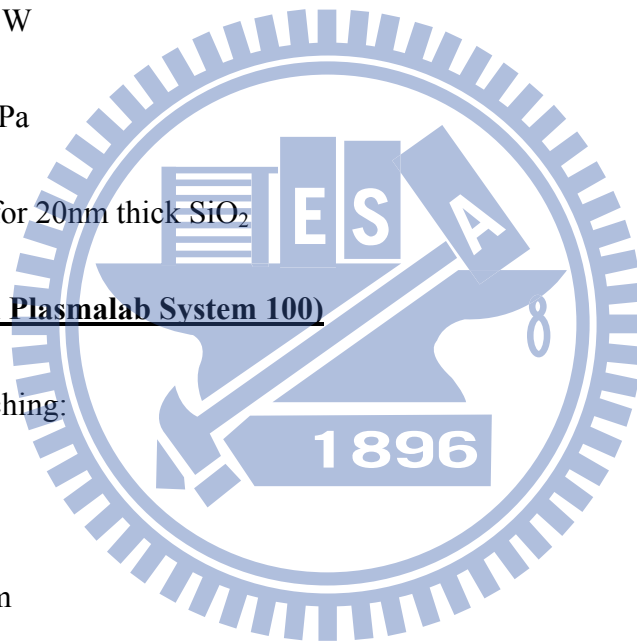
Pressure: 7.5x10⁻⁹Torr

Temperature: 20°C

Time: 3min. 40sec. to etch 300nm thick Si₃N₄ film

ICP-RIE (SAMCO RIE-101PH)

- GaN film etching:



Cl₂: 25sccm

Ar: 10sccm

ICP Power: 200W

Bias Power: 200W

Pressure: 0.33Pa

Time: 55sec. to etch 500nm thick GaN film

E-beam Lithography System (JEOL JSM-6500)

- Spin coating use PMMA (A5)

First step: 1000 rpm for 10sec.

Second step: 3500 rpm for 25sec.

- Hard bake: hot plate 180°C, 90sec.

- Exposure:

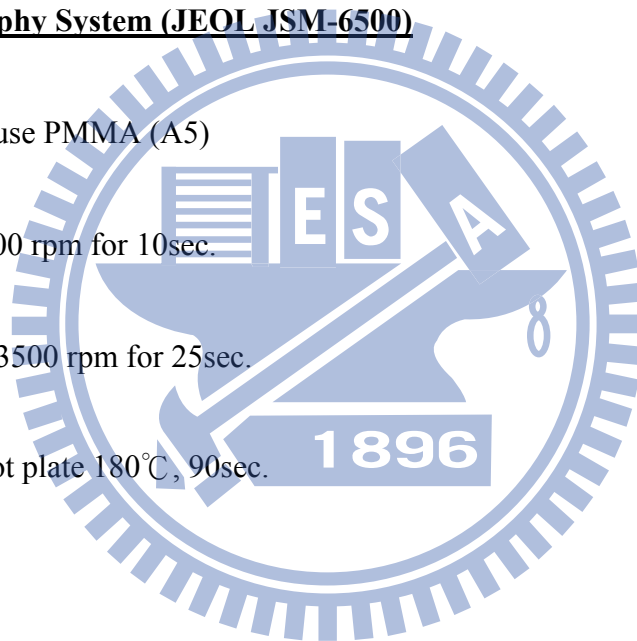
Beam voltage: 25KeV

Dosage: 1.4~1.7 (point does)

- Development: MIBK: IPA (1:3) 70sec.

- Fixing: IPA 40sec.

E-gun Evaporation System (ULVAC EBX-8C)



- Source: Aluminum
- Pressure: 3×10^{-6} Torr
- Current: 170mA for first 5nm

200mA for the rest 55nm

- Pressure: 3×10^{-6} Torr

3.2 Lasing Characteristics of Metal-coated GaN Nanostripe at Room Temperature

To explore experimentally about our device, we use the micro-Photoluminescence system mentioned in the previous chapter to measure its characteristics. We pump our device directly from the metal side to avoid the absorption of undoped GaN layer beneath our device, if we choose to pump the device from the back of the wafer.

First, to ensure that the lasing action is truly originated from our nano structure, we use a He-Cd 325nm continuous-wave laser to pump the flat region of undoped GaN layer, before and after the deposition of dielectric layer and metal to see the Photoluminescence (PL) spectrum of them. As shown in Fig. 3.2.1, the peak wavelength of undoped GaN layer is about 362nm. However, the spectrum after the deposition of SiO₂ and aluminum layer is totally different, the peak around 362nm no longer exists because the energy from 350nm to 380nm had been totally absorbed by shielding layer. Therefore, we could use Fig. 3.2.1 to prove that the lasing action is truly from our nano structure. Moreover, from Fig. 3.2.2, the

PL spectrum of the metal-coated nanostripe below (black) and above (red) the threshold power density has been presented. This device has a single lasing mode at 370nm and the difference between two spectrums further ensure that we observe a lasing action in our structure. From the light-in light-out curves of this mode shows in Fig. 3.2.3 and the linewidth of the lasing mode, we could observe linear behavior after soft turn-on which indicates the lasing action, and also the narrowing linewidth shows that the transition from spontaneous emission to stimulated emission of the optical mode. These evidences prove the lasing action in our metal-coated GaN nanostripe. The threshold pump power density is about 0.055kW/cm^2 (55mJ/cm^2) and the quality factor estimated by the wavelength to linewidth around the transparency is 150. Compared to the sample without metal or SiO_2 shielding layer, the high thermal conductivity and high reflectivity of aluminum make measurement easier and increase the possibility of lasing at room temperature. Moreover, the SiO_2 layer would passive the surface roughness created by the dry etching processes and therefore reduce the nonradiative center on the surface of the nanostripe, and it reduce energy loss if the metal layer is directly coated on to the gain medium, this would reduce the absorption and lower the threshold gain of this device, making lasing action possible [1].

The nanostripe without shielding layer exhibits high optical loss and lower Q value. It was for these reasons that we can't observe lasing action in uncoated GaN nanostripe. The reason why we use aluminum instead of other metal like silver or gold to form our

metal-coated device is that aluminum has a higher reflectivity which could show a better optical confinement at UV wavelength region compared with silver [2], even aluminum is also quite lossy at this wavelength region. Also, the adhesive ability to SiO₂ is better for aluminum than gold.

3.3 Simulation Results and Discussion

To get a better understanding of our experiment results, we use finite-element-method (FEM) to simulate the optical mode in our metal-coated nanocavity. The simulation model consists of a sapphire layer, an undoped GaN layer, a thin SiO₂ layer, and an aluminum shielding layer. The refractive indexes of aluminum and undoped GaN layers established by Peng and Piprek [3], and Rakic *et al.* [4], with the refractive index of the SiO₂ are 1.46. This model also includes a perfectly matched layer surrounds the nanocavity to absorb redundant signal which might reflect back to the metal-coated nanocavity, thereby influencing the simulation result. Fig.3.3.1 shows the simulated optical mode profiles for a GaN nanostripe cavity with or without the shielding layers. In Fig.3.3.1 (a), the model incorporating metal and SiO₂ layers had an optical mode well confined within the nanostripe, demonstrating a clear standing wave pattern with 3.5 nodes. However, for the nanostripe without shielding layers in Fig. 3.3.1 (b), the optical mode leaks into the region of air with a standing wave pattern lacked uniformity, compares with the metal-coated nanostripe. The wavelength of the optical mode shown in Fig. 3.3.1 (a) is 367nm, and the quality factor is about 150, which is

ten times larger than the case in Fig. 3.3.1 (b). This illustrates the difficulty of achieving GaN nanostripe lasing without dielectric and metal layer coated on it. The small differences between the experimental and simulation results might come from the imprecise fabrication processes and the imprecision of material indices used in the simulation model. From the discussion above, we confirmed that the metal shielding layer in this structure plays an important role in lasing at room temperature. And also, from the thermal conductivity of aluminum (237W/m-k) and air (0.025W/m-k), it indicates that under room temperature pulsed condition, metal-coated nanostripe has a better opportunity to observe lasing action before it breaks down than the nanostripe without shielding layers.

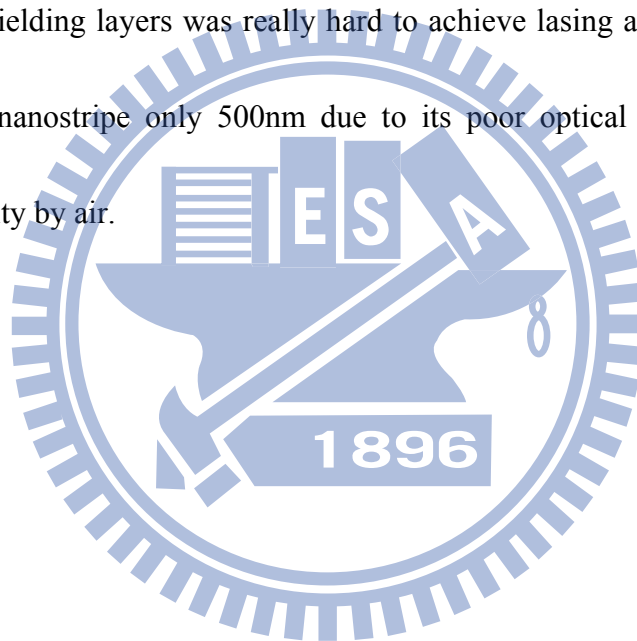
To further improve the performance of this device, vertical confinement would be the key issue. Distributed Bragg Reflector (DBR) would significantly reduce the energy loss from the bottom of the nanostripe as shown in Fig. 3.3.1 (a). For example, C. Y. Lu *et al.* demonstrated this idea by an n-type DBR with metal coated on the microrod [5]. The device operated under room temperature continuous-wave condition, and showed a high thermal resistance. This would form a three dimensional cavity which would definitely improve the performance of the device and even operate under electrically pumped condition. Also, heterostructure with precise calculation to confine the optical field in the active region would also work [6].

Moreover, we adopt effective index method to calculate the band diagram of this structure. The effective index method is an efficient method to analysis rectangular waveguide structure, which is really common structure for semiconductor laser. The ridge waveguide structure has been split into different part first, and calculates the effective indexes of each part, then combined these parts together again and calculate the true effective index of this structure. A representation schematic diagram is shown in Fig. 3.3.2. This way put the complex two dimensional calculations into one dimensional, and still keeps a high accuracy with the experimental result. In our case, we split our nanostripe structure into three parts as shown in Fig. 3.3.3 and then calculate the band diagram. The TE mode band diagram is shown in Fig. 3.3.4, as you could see, there is only one waveguide band in this structure. Moreover, around 370nm there is waveguide mode quite fit to our experimental result. We believe that the single mode lasing we observe in the experiment is a combination of TE waveguide mode with surface plasmon mode from the Al/SiO₂/GaN interfaces. The calculation helps us to clarify the observation result and further prove that there would be only one optical mode with a clear standing wave pattern confine in the nanostripe, which makes lasing action possible.

3.4 Summary

In sum, we demonstrated lasing in metal-coated GaN nanostripe at room temperature pulse condition with the width of the nanostripe is only about 500nm. Lasing wavelength

was about 370nm and the threshold power density is about 0.055kW/cm². The quality factor was about 150 estimated from the experimental result. FEM simulation result showed the importance of aluminum layer coated on the nanostripe in the lasing action, and from effective index method, the single mode lasing was confirmed by the band diagram of the nanostripe structure, which had only one waveguide band around 300nm to 400nm wavelength region. From experimental and simulation results, the GaN nanostripe without metal and SiO₂ shielding layers was really hard to achieve lasing at room temperature with the width of the nanostripe only 500nm due to its poor optical confinement and worse thermal conductivity by air.



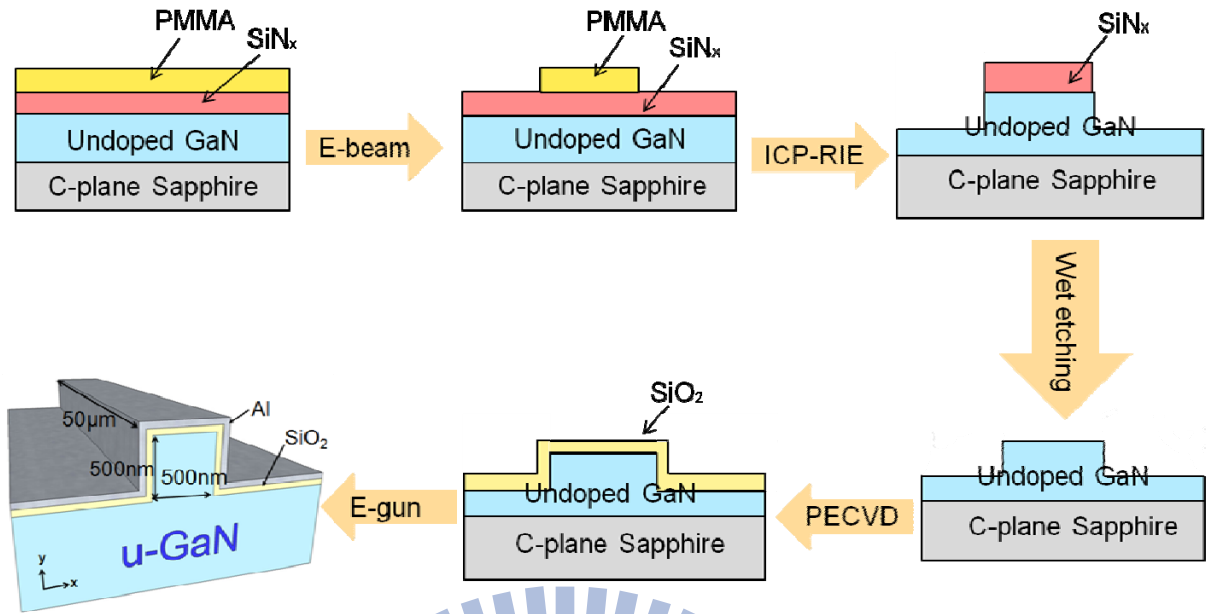
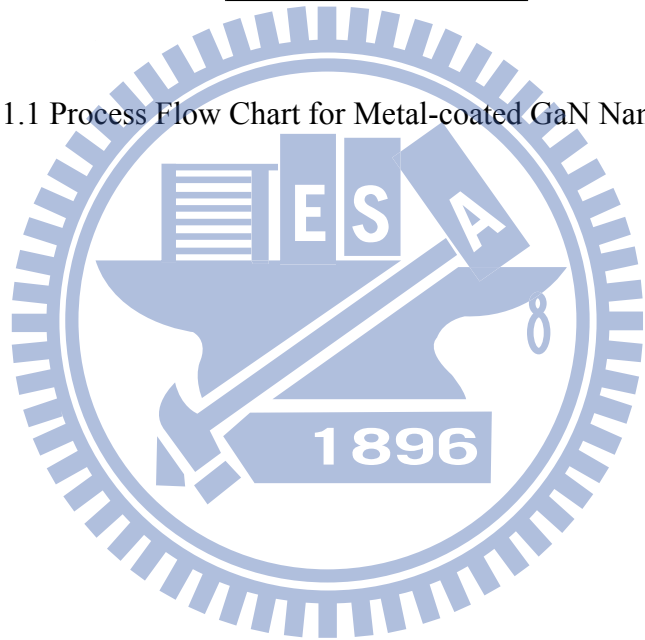


Fig. 3.1.1 Process Flow Chart for Metal-coated GaN Nanostripe.



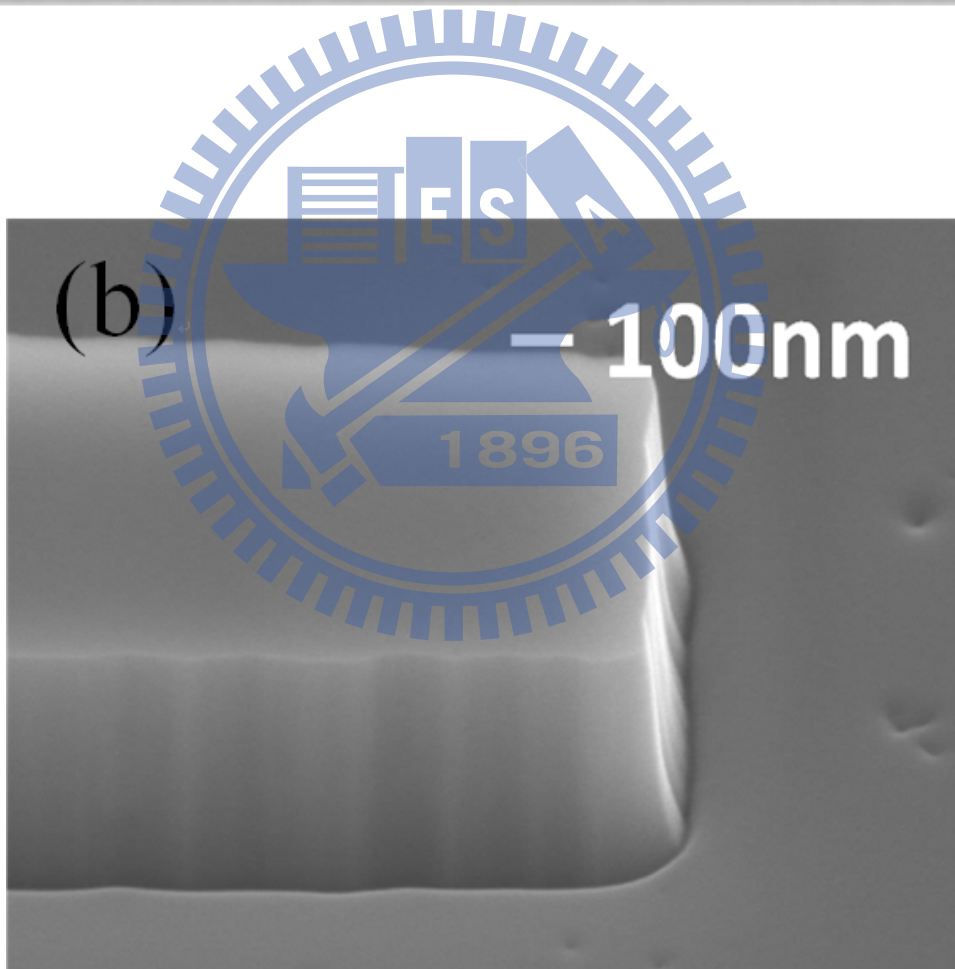
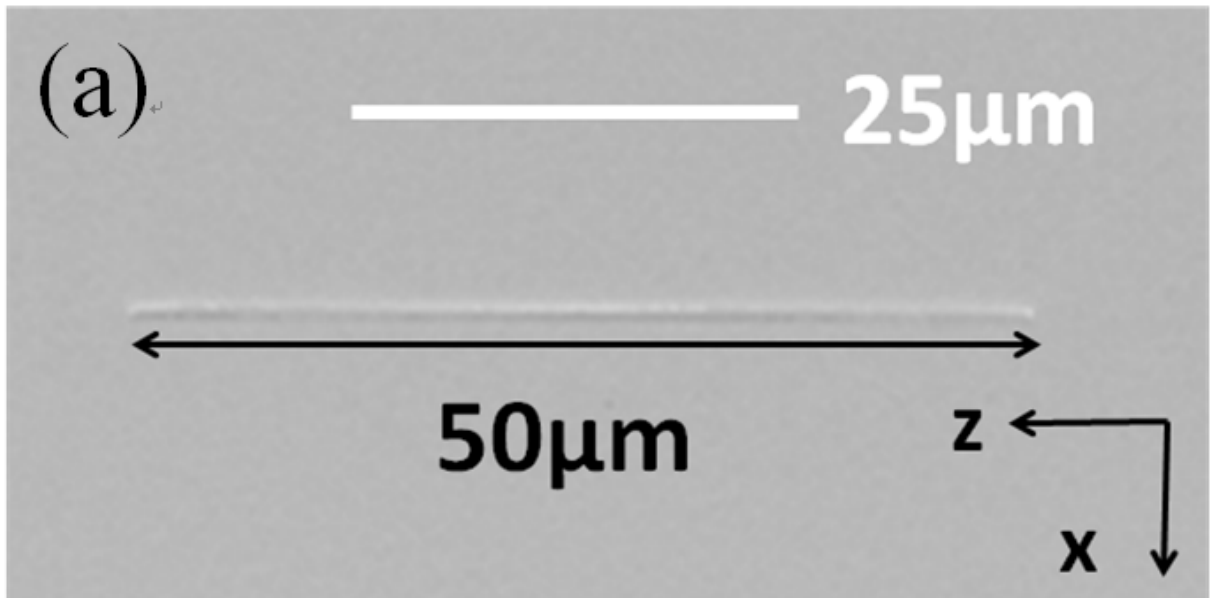


Fig. 3.1.2 SEM Image of Metal-coated GaN Nanostripe (a) Top View of the GaN Nanostripe before Deposition of Shielding Layers. (b) Angle View of One side of the GaN Nanostripe before Deposition of Shielding Layers.

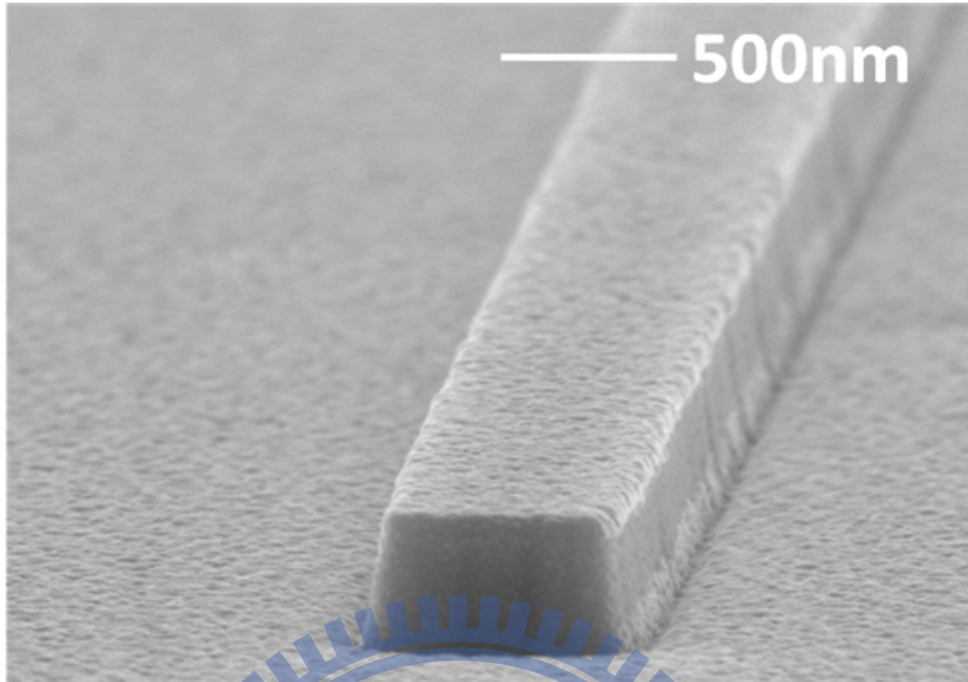


Fig. 3.1.3 Angle View of the GaN Nanostripe after the Deposition of SiO₂ and Aluminum Layers.

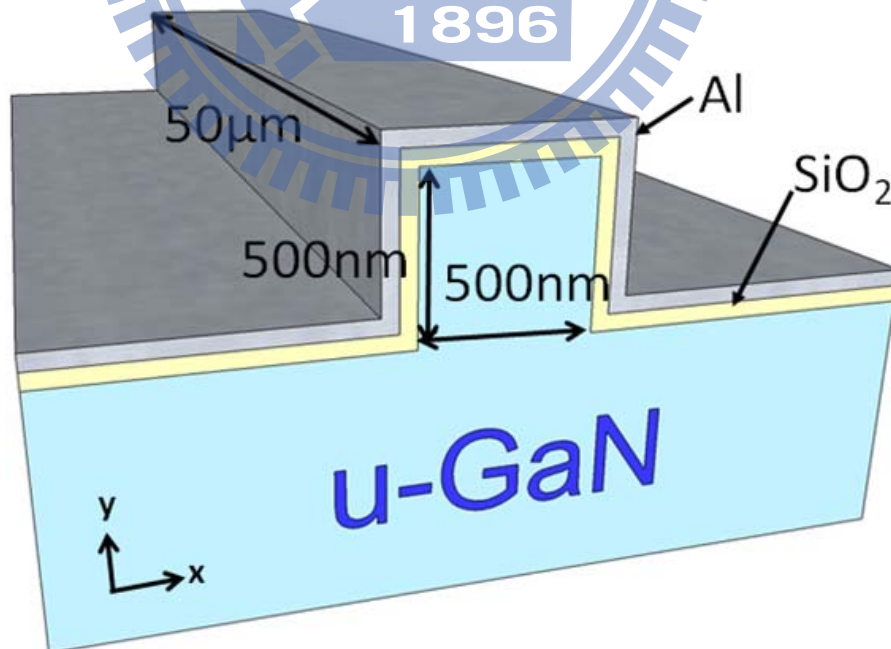


Fig. 3.1.4 Schematic Diagram of Metal-coated GaN Nanostripe.

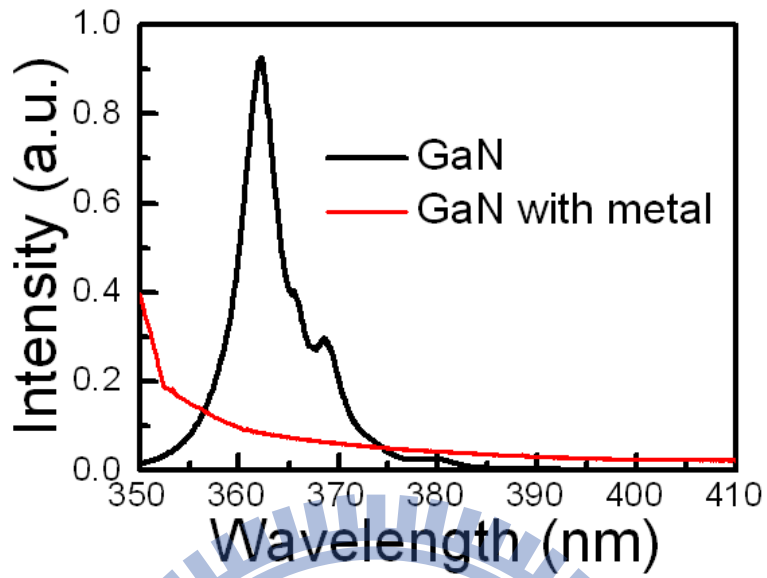


Fig. 3.2.1 PL Spectrum of Undoped GaN Layer with and without Metal and Dielectric Shielding Layers.

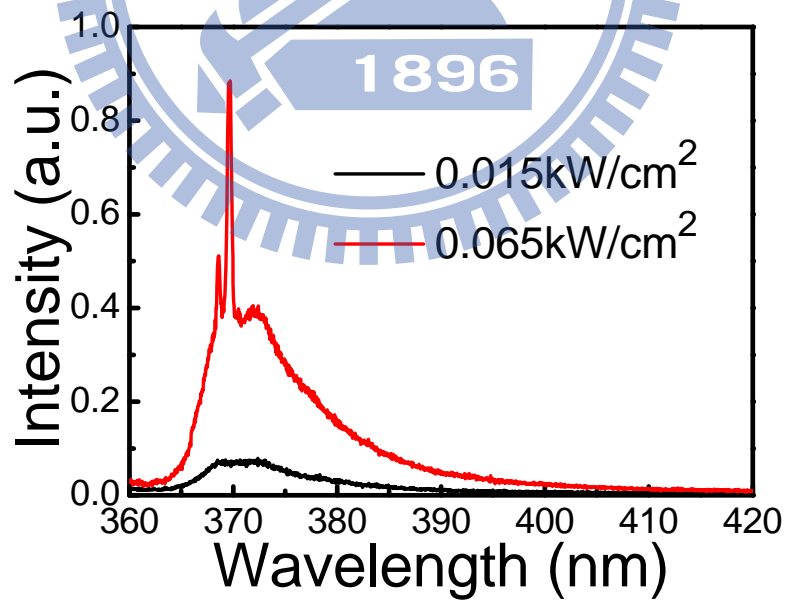


Fig. 3.2.2 PL Spectrum of Metal-coated GaN Nanostripe Above (Red) and Below (Black)

Threshold.

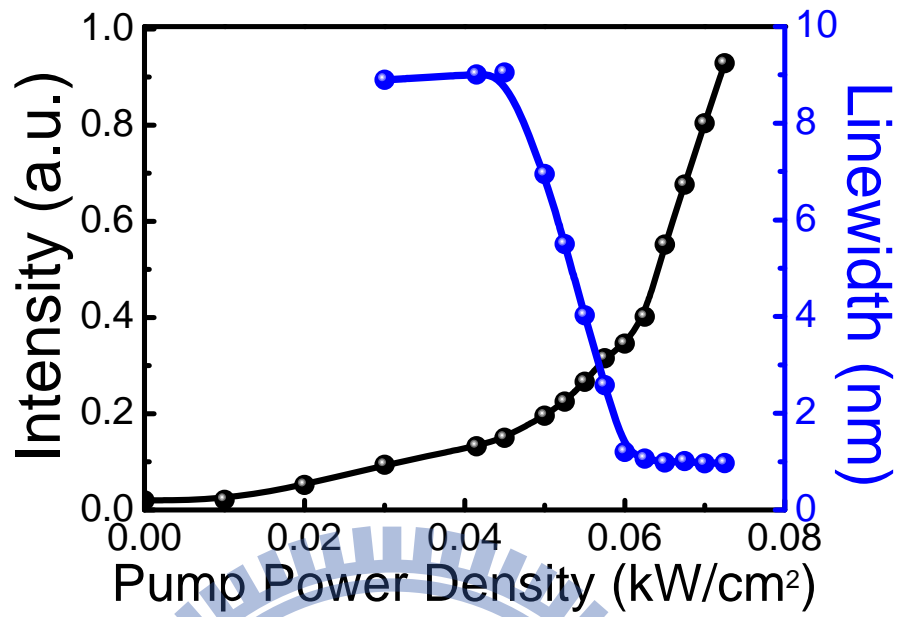
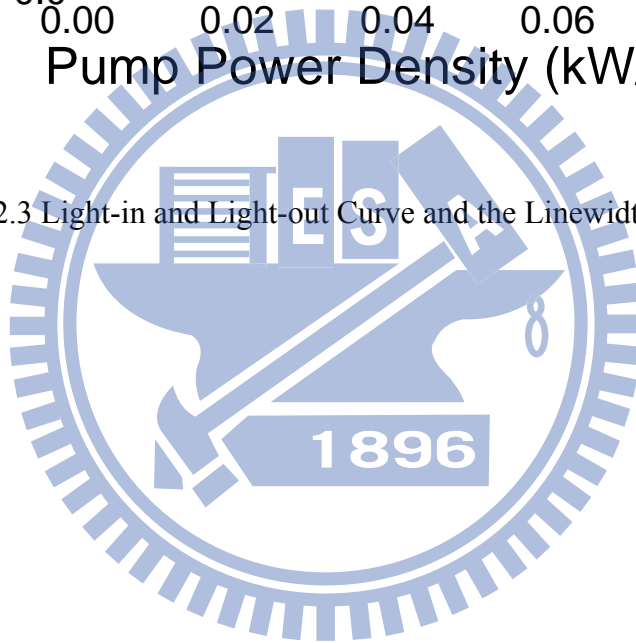


Fig. 3.2.3 Light-in and Light-out Curve and the Linewidth of Lasing Peak.



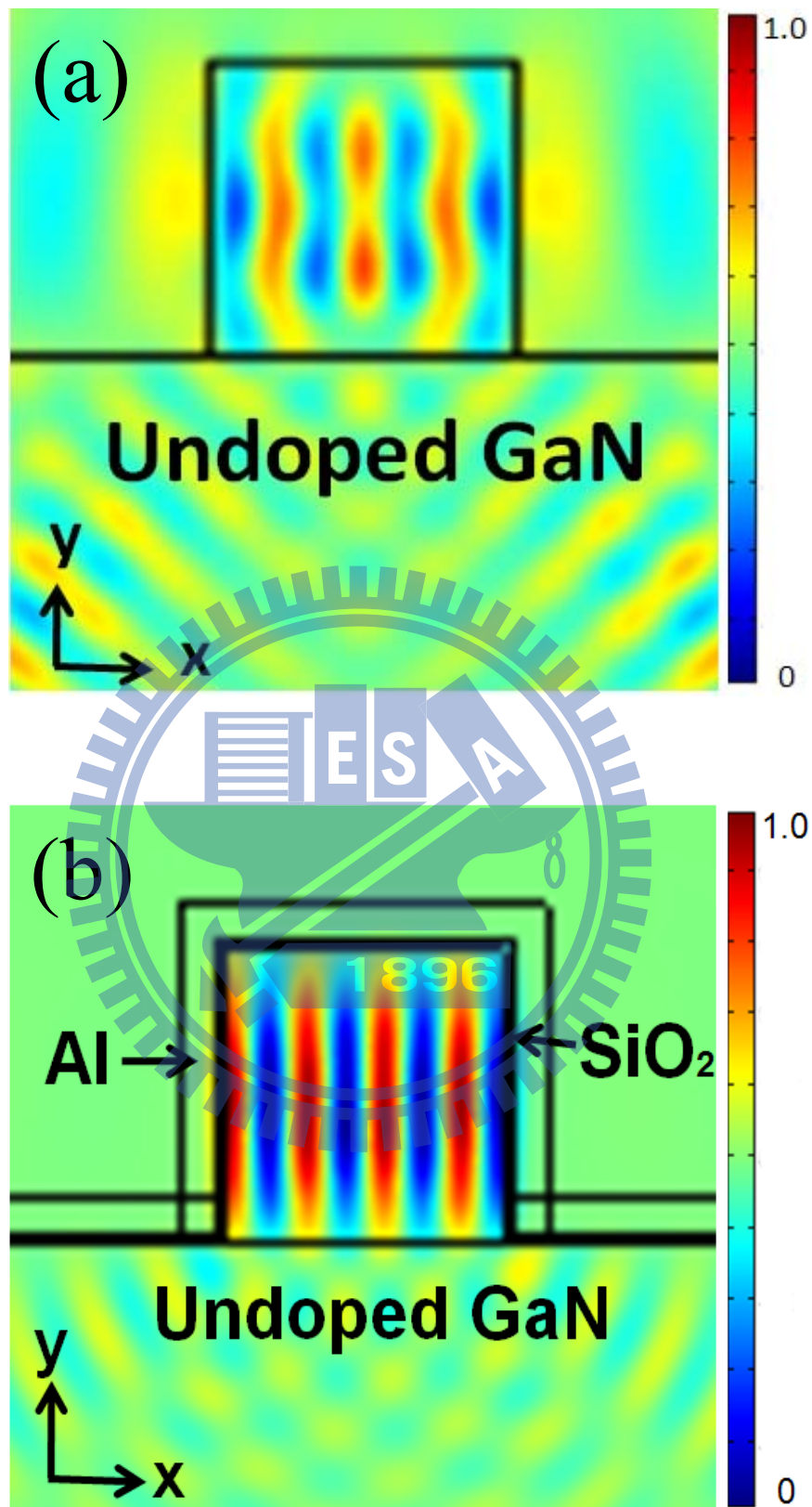


Fig.3.3.1 (a) The E_z Mode Profile of the Nanostripe without Shielding Layers. (b) The

The E_z Mode Profile of the Nanostripe with Shielding Layers.

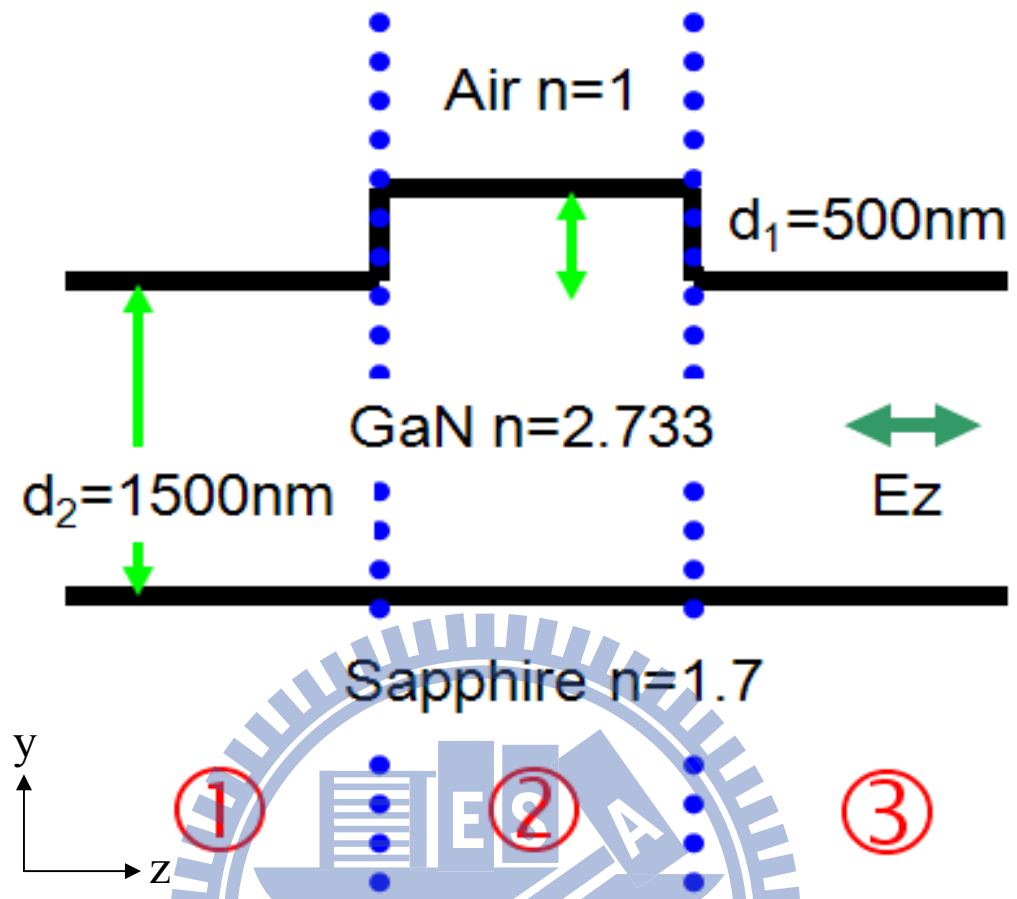


Fig. 3.3.2 Schematic Diagram of the Nanostripe Model in Effective Index Method.

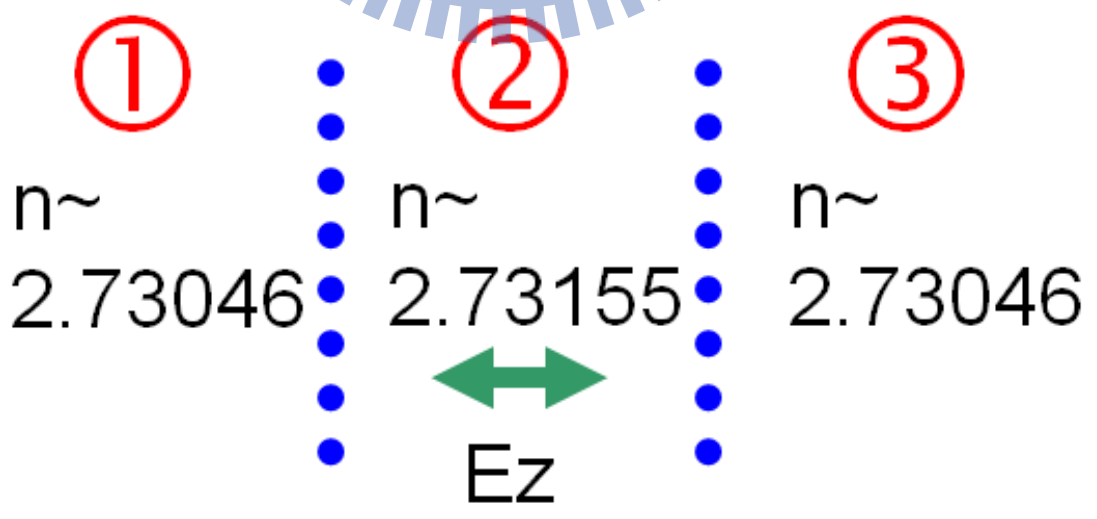


Fig. 3.3.3 Effective Structure of Nanostripe under TE Mode.

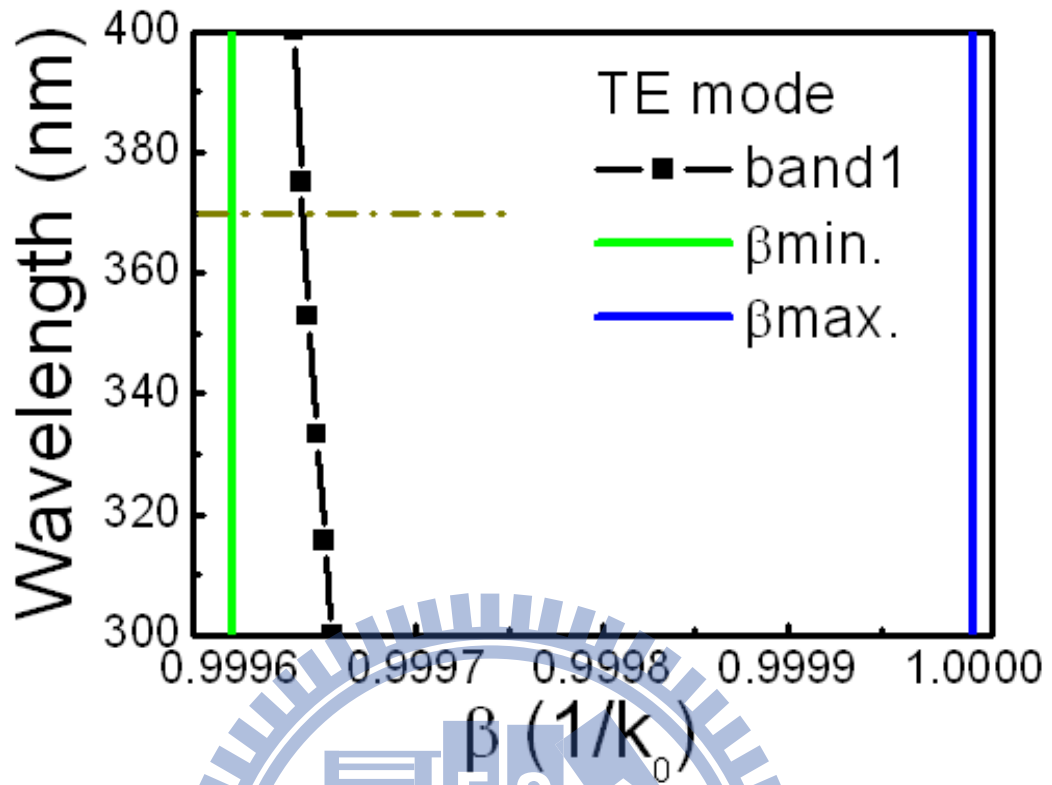


Fig. 3.3.4 TE Mode Band Diagram of Nanostripe.

References:

- [1] A. Mizrahi, V. Lomakin, B. A. Slutsky, M. P. Nezhad, L. Feng, and Y. Fainman, "Low threshold gain metal coated laser nanoresonators," *Opt. Lett.*, vol. **33**, pp. 1261, 2008.
- [2] W. M. Rohsenow and H. Choi, "Heat Mass and Momentum Transfer," Prentice Hall, New York, (1961).
- [3] T. Peng, and J. Piprek, "Refractive index of AlGaInN alloys," *Electron. Lett.*, vol. **32**, pp. 2285, 1996.
- [4] A. D. Rakic, A. B. Djuricic, J. M. Elazer, and M. L. Majewski, "Optical properties of metallic films for vertical-cavity optoelectronic devices," *Appl. Opt.*, vol. **37**, pp. 5271, 1998.
- [5] C. Y. Lu, S. W. Chang, S. L. Chuang, T. D. Germann, and D. Bimberg, "Metal-cavity surface-emitting microlaser at room temperature," *Appl. Phys. Lett.*, vol. **96**, pp. 251101, 2010.
- [6] M. T. Hill, "Status and prospects for metallic and plasmonic nanolasers," *J. Opt. Soc. Am. B*, vol. **27**, pp. B 36, 2010.

Chapter 4 Lasing in Metal-coated GaN Nanoring at Room Temperature

4.1 Epitaxial Characteristics and Fabrication Process of Metal-coated GaN Nanoring

We use undoped GaN layer grown on C-plane (0001) sapphire substrate as gain medium. The thickness of the undoped GaN layer is about 2 μ m. Metal-organic chemical vapor deposition (MOCVD) system (EMCORE D-75) is used to grow undoped GaN layer on the polished optical-grade C-plane (0001), 2 inches sapphire substrate. Trimethylgallium (TMGa) and Ammonia (NH₃) were used as the Ga and N sources respectively.

First, a thermal cleaning process was carried out at 1080°C for 10 minutes in a stream of hydrogen ambient before the growth of epitaxial layers to clean the sample surface. Second, the 30nm thick GaN nucleation layer was first grown on the sapphire substrate at 530°C, and at the end the 2 μ m thick undoped GaN layer was grown on it at 1040°C.

After we finish the preparation of sample, we adopt some fabrication processes to complete our device. The complete process flow chart for our device is shown in Fig. 4.1.1.

First, we deposit 300nm thick Si₃N₄ layer on the undoped GaN layer as an etching mask for the following E-beam lithography process. Second, for E-beam lithography process, we use spin coater to put a thin polymethylmethacrylate (PMMA) on the sample, then the nanostripe pattern was defined using E-beam lithography system. After this, we use ICP-RIE dry etching system to transfer the pattern on the PMMA layer onto the Si₃N₄. And the transfer the pattern again onto the undoped GaN layer to form the nanostripe structure on it. Fig.

4.1.2 shows the SEM images of different size of nanorings from angled view after these processes.

Third, before we start to do the next step, we use wet etching method to clean our sample, washing away the particles created in the previous dry etching processes to promote the performance of our device. After this, we use E-gun evaporation to deposit a 50nm thick aluminum layer to complete our device. Fig. 4.1.3 shows one of the nanorings after metal deposition. The detail recipe of each process is shown in the following paragraphs, and the schematic diagram of metal-coated GaN nanoring is shown in Fig. 4.1.4.

PECVD (SAMCO PD220)

- Si_3N_4 film deposition:

SiH_4/Ar : 20sccm

NH_3 : 10sccm

N_2 : 490sccm

Temperature: 300°C

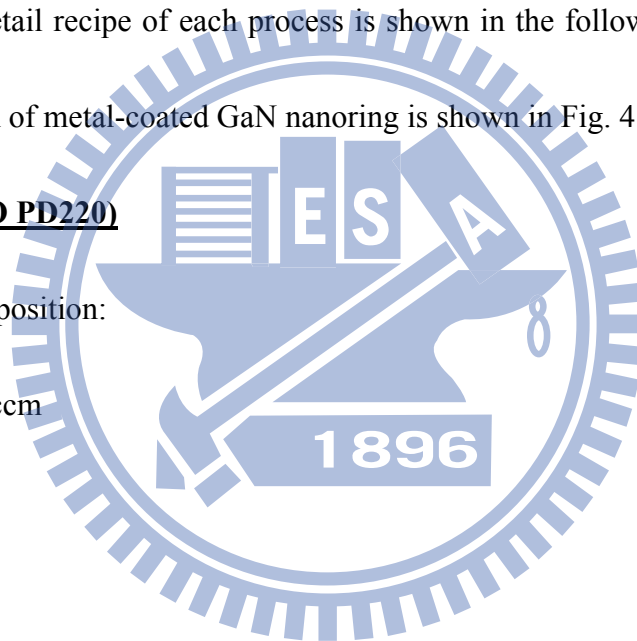
RF Power: 35W

Pressure: 100Pa

Time: 31 min for 300nm thick Si_3N_4

ICP-RIE (Oxford Plasmalab System 100)

- Si_3N_4 film etching:



Ar/O₂: 5sccm

CHF₃: 50sccm

RF Power: 150W

Pressure: 7.5×10^{-9} Torr

Temperature: 20°C

Time: 3min. 35sec. to etch 300nm thick Si₃N₄ film

ICP-RIE (SAMCO RIE-101PH)

- GaN film etching:

Cl₂: 25sccm

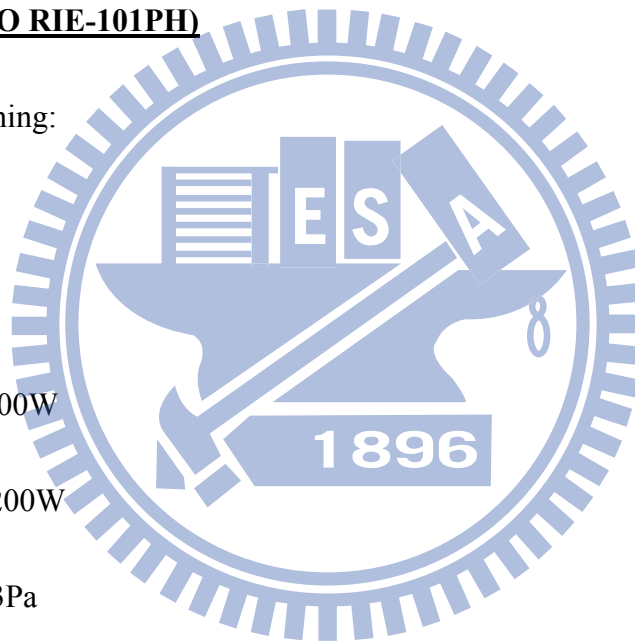
Ar: 10sccm

ICP Power: 200W

Bias Power: 200W

Pressure: 0.33Pa

Time: 65sec. to etch 600nm thick GaN film



E-beam Lithography System (JEOL JSM-6500)

- Spin coating use PMMA (A5)

First step: 1000 rpm for 10sec.

Second step: 3500 rpm for 25sec.

- Hard bake: hot plate 180°C, 90sec.

- Exposure:

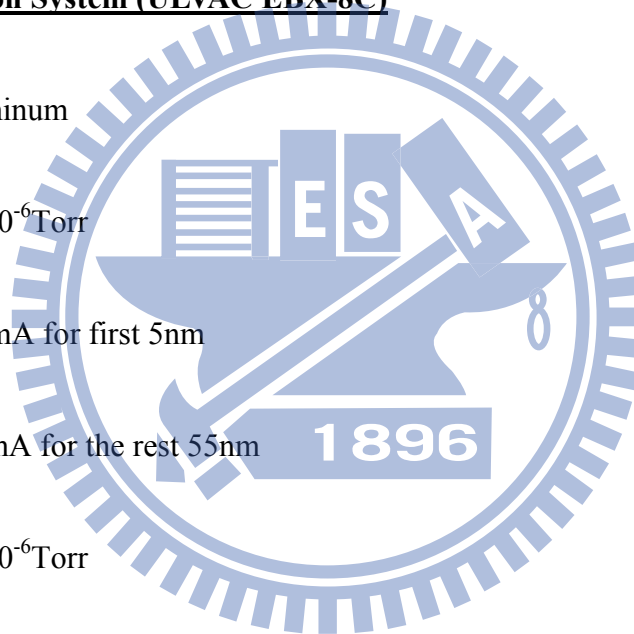
Beam voltage: 25KeV

Dosage: 1.4~1.7 (point does)

- Development: MIBK: IPA (1:3) 70sec.
- Fixing: IPA 40sec.

E-gun Evaporation System (ULVAC EBX-8C)

- Source: Aluminum
- Pressure: 3×10^{-6} Torr
- Current: 170mA for first 5nm
200mA for the rest 55nm
- Pressure: 3×10^{-6} Torr



4.2 Lasing Characteristics of Metal-coated GaN Nanoring at Room Temperature

To investigate the performance of our metal-coated GaN nanoring device, we use the micro-Photoluminescence system mentioned in chapter 2 to measure the lasing characteristics of our devices. We directly pump our device at room temperature, trying to avoid absorption loss from the undoped GaN layer which is beneath our nanoring structure.

In our experiment, there are three different sizes of nanoring structure: $7\mu\text{m}$, $5\mu\text{m}$, and $3\mu\text{m}$ in diameter. Fig. 4.2.1 to Fig. 4.2.3 shows the lasing characteristics of metal-coated nanorings with different diameter. The smallest nano structure we observe lasing action is the nanoring structure with $3\mu\text{m}$ in diameter, 600nm in height, and 310nm in width. The width of this structure is below the nature wavelength of the lasing mode. Due to better control of dry etching processes, there is no SiO_2 layer between metal and gain medium for nanoring structure, trying to utilize the advantages of surface plasmon effect as much as possible. Following paragraphs are the lasing characteristics of our nanoring devices.

For metal-coated GaN nanoring with $7\mu\text{m}$ in diameter, we observe a lasing action with lasing wavelength around 365nm , which is shown in Fig. 4.2.1 (a). The spectrum above (red) and below (black) the threshold for our nano structure clearly indicate that we observe a lasing action. From Fig. 4.2.1 (b), the threshold pump power density is 0.019 kW/cm^2 (19mJ/cm^2) obtained from the experimental result. Moreover, the quality factor estimated by the ratio of wavelength to linewidth around the transparency is about 910. We believe this high quality factor could attribute to the combination of whispering-gallery mode and surface plasmon mode. This is the reason why we could still observe lasing action even though we shrink the size of our device to a smaller scale.

We further shrink the diameter of the nanoring to $5\mu\text{m}$, and the width of the nanoring to 340nm . The width of the nanoring is smaller than the lasing wavelength. The lasing

characteristics are shown in Fig. 4.2.2. The lasing peak is around 363nm, as we could see that the spectrum above and below the threshold for this structure is quite different. For this case, the threshold pump power density is about $0.042\text{kW}/\text{cm}^2$ ($42\text{mJ}/\text{cm}^2$), and the quality factor is about 910, which is quite the same as the result of metal-coated GaN nanoring in the previous paragraph. Clear turn-on behavior of L-L curve and the narrowing linewidth of the lasing peak after turn-on both indicate the lasing action at room temperature.

At last, the smallest nanoring structure which we could observe lasing action at room temperature is $3\mu\text{m}$ in diameter, 600nm in height, and 310nm in width. It is the best result we could obtain under room temperature, pulsed condition. For this case, the lasing wavelength is 364nm and the quality factor is about 800. The difference in quality factor of our device might be due to the smaller device, the stronger interaction between metal and gain medium is under such a small scale. The threshold pump power density is around $0.045\text{kW}/\text{cm}^2$ ($45\text{mJ}/\text{cm}^2$) estimated from the L-L curve shown in Fig. 4.2.3 (b). The increase in threshold power density might be due to the beam spot size of our micro-PL system is about $50\mu\text{m}$, which is much larger than the nanoring device. Poor injection efficiency might be the reason for increasing threshold power when we have smaller device. Table 4.2 shows the lasing characteristics and the geometric parameter of our device.

4.3 Result and Discussion

Compare to the nanostripe structure, nanoring structure has a unique advantage that

utilize whispering-gallery mode which do not require other feedback structure to form the cavity [1]. Therefore, metal layer coated on the nanoring structure could be specifically used to reduce optical loss from the side of the nanoring structure and makes lasing action possible at room temperature. Higher quality factor is expected for nanoring structure compare to waveguide structure. Higher quality factor indicates that photon in this structure would stay longer and have higher chance to get enough gain from the gain medium to overcome the loss. The experiment result of metal-coated GaN nanoring laser confirms our hypothesis. Even though both nano structures are benefit from better optical confinement and better thermal conductivity which make lasing action possible at room temperature, the advantages of whispering-gallery-mode make the device performance of nanoring better than nanostripe structure. Moreover, these advantages let us could shrink our device to smaller scale compare to the nanostripe structure. We could still observe lasing action at room temperature with the width of the nanoring down to subwavelength scale, which is not possible for nanostripe case.

Table 4.3 lists a comparison between nanostripe and nanoring structure.

As shown in the Table 4.3, the size of the nano structure has reduced significantly. Compare to nanostripe structure, which has a size about $12.5\mu\text{m}^3$, the size of the smallest nanoring structure we could observe lasing action at room temperature is $1.7\mu\text{m}^3$, seven times smaller than the nanostripe structure. Moreover, the width of the nanoring has been shrunk down to 310nm, which is smaller than the lasing wavelength we observe. We could not

achieve lasing in such a thin structure in nanostripe case. We believe that the utilization of whispering-gallery mode would be the key reason for this result.

Moreover, compare to the lasing characteristics of these two devices, the nanoring structure has a lower threshold power density and higher quality factor. The quality factor is about 6 times larger for nanoring structures which are 5 or 7 μm in diameter, and about 5.5 times for nanoring structure which is 3 μm in diameter. The threshold power density is at least 20% lower for the nanoring structure compare to the nanostripe structure.

In conclusion, whispering gallery mode would be a better choice to further improve the performance of metal-coated nanocavity than fabry-perot oscillation from the waveguide structure.

4.3 Summary

Even though some research results about metal-clad microring laser already reported experimentally and theoretically [1,4], they only observed lasing action at 77K and the quality factor was about 160, which was quite similar to other structure reported previously [5-7]. The advantages of whispering-gallery mode weren't fully utilized by them. Therefore, in our experiment, we demonstrate lasing in metal-coated GaN nanoring at room temperature. It is the first time in the world that demonstrates lasing in metal-coated nanoring cavity at room temperature with GaN-based material system with such a high quality factor.

In our experiment, we fabricate three different size of the device: 7 μm , 5 μm , and 3 μm in

diameter. They all could observe lasing action at room temperature by optical pumping. Besides, their quality factors are about 800 to 900, much higher than previous reported data. The lasing wavelength of each device is 365nm, 363nm, and 364nm, and the threshold power density for each one is $0.019\text{kW}/\text{cm}^2$ ($19\text{mJ}/\text{cm}^2$), $0.042\text{kW}/\text{cm}^2$ ($42\text{mJ}/\text{cm}^2$), and $0.045\text{kW}/\text{cm}^2$ ($45\text{mJ}/\text{cm}^2$) respectively.

Compare to the nanostripe structure mentioned in the previous chapter, nanoring structure has higher quality factor and lower threshold power density than it. We could further shrink the volume of the device to one tenth the nanostripe structure, and the width of the nanoring is smaller than the lasing wavelength. We attribute this result to better feedback mechanism brought by nanoring structure. Moreover, from the experimental result, the red-shift of lasing peak wavelength of the reference sample compares to the metal-coated one which shows a steady blue-shift as pumping power increase indicates that metal could provide better thermal dissipation than the air, so the device's performance won't be influenced by heat even operate at high power density.

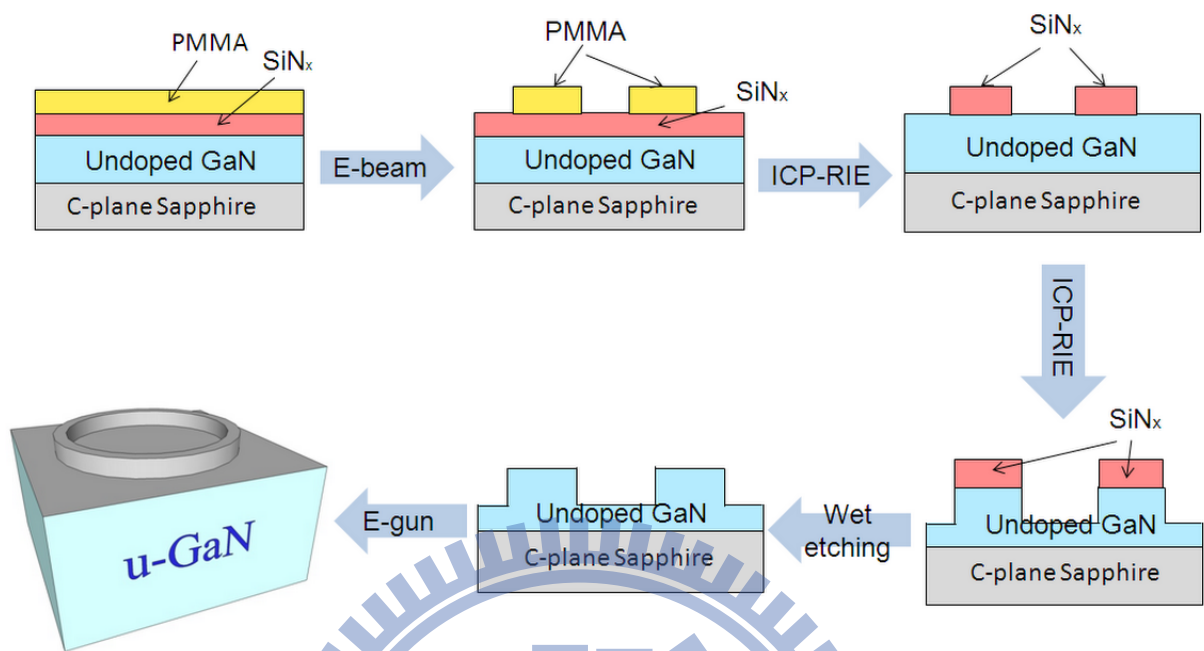
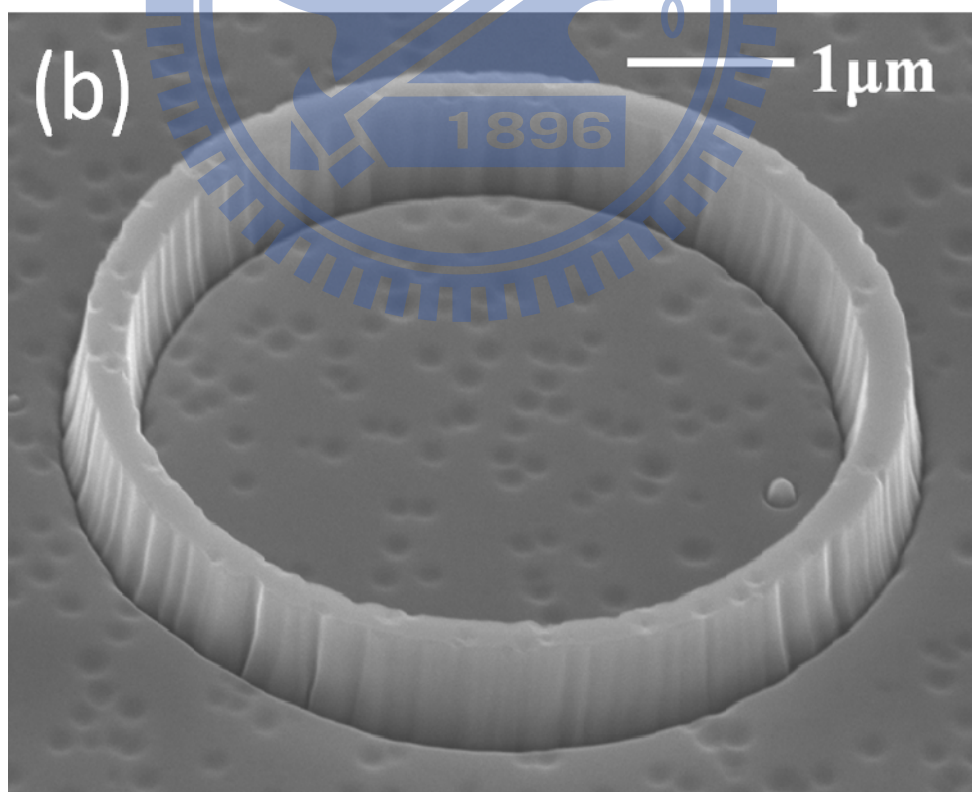
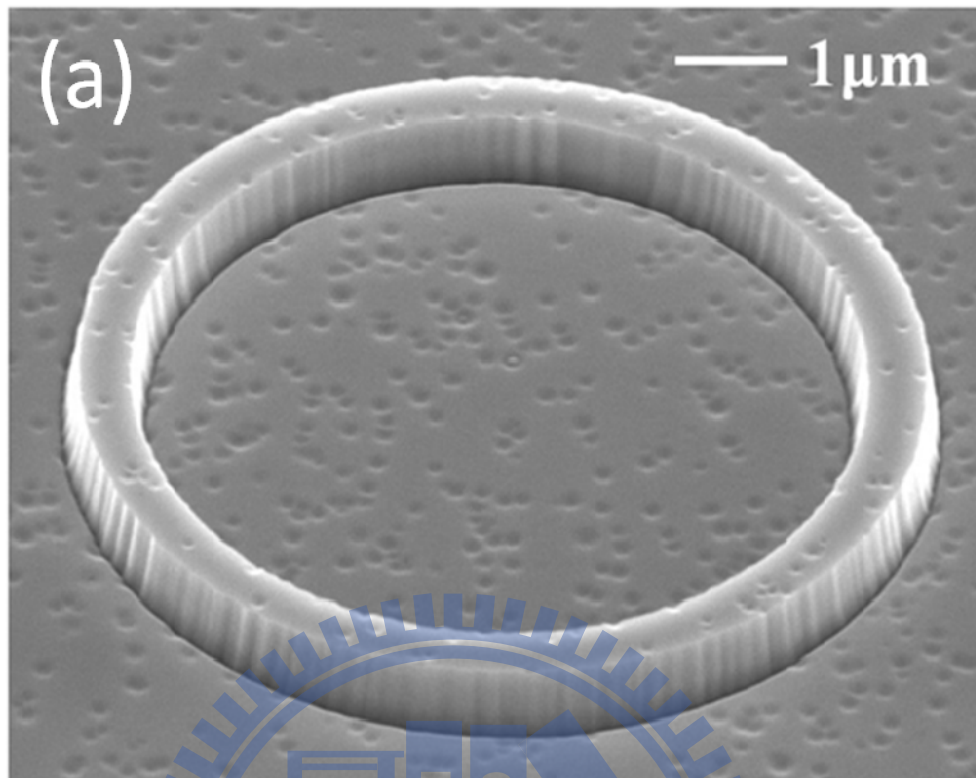


Fig. 4.1.1 Process Flow Chart for Metal-coated GaN Nanoring.



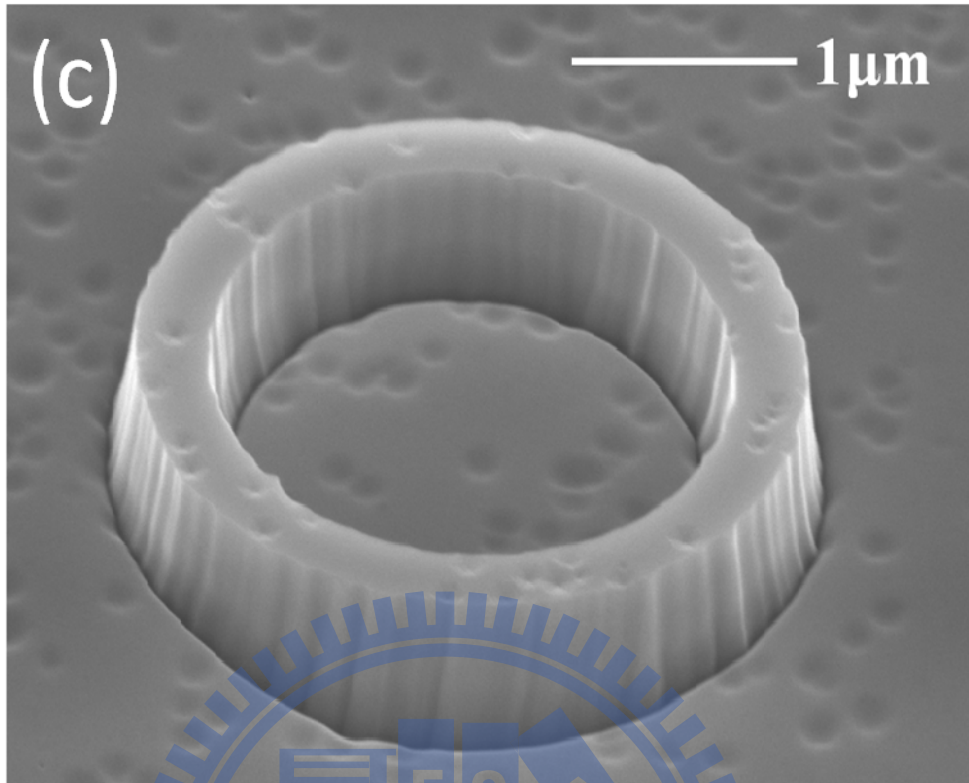


Fig. 4.1.2 SEM Image of Different Size of GaN Nanoring before Shielding Layer Deposition (a) 7 μm in diameter. (b) 5 μm in diameter. (c) 3 μm in diameter.

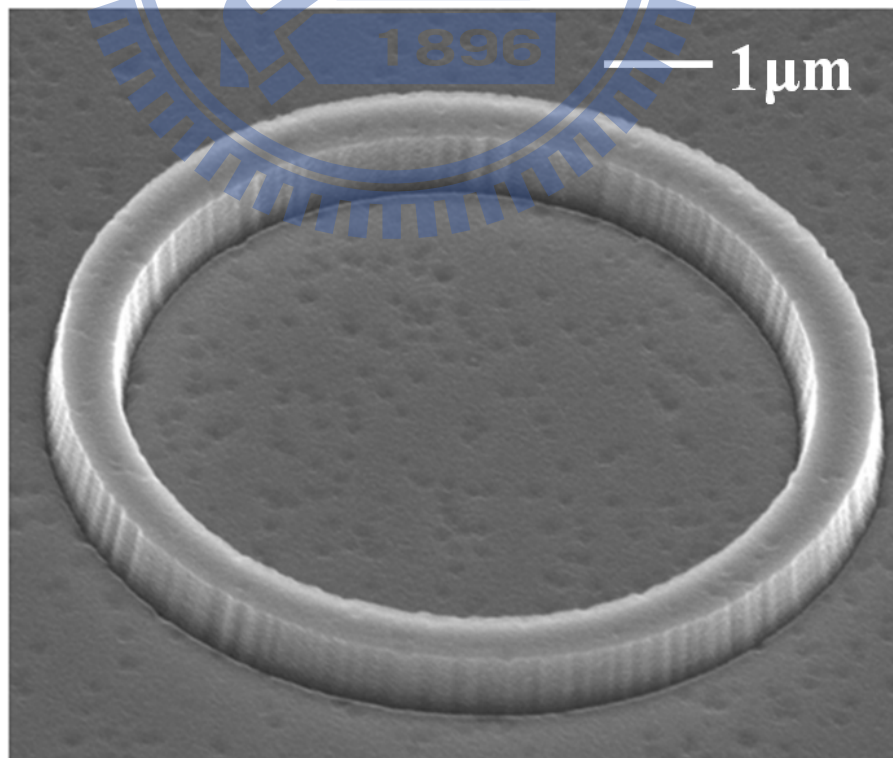


Fig. 4.1.3 SEM image of metal-coated GaN nanoring, 7 μm in diameter.

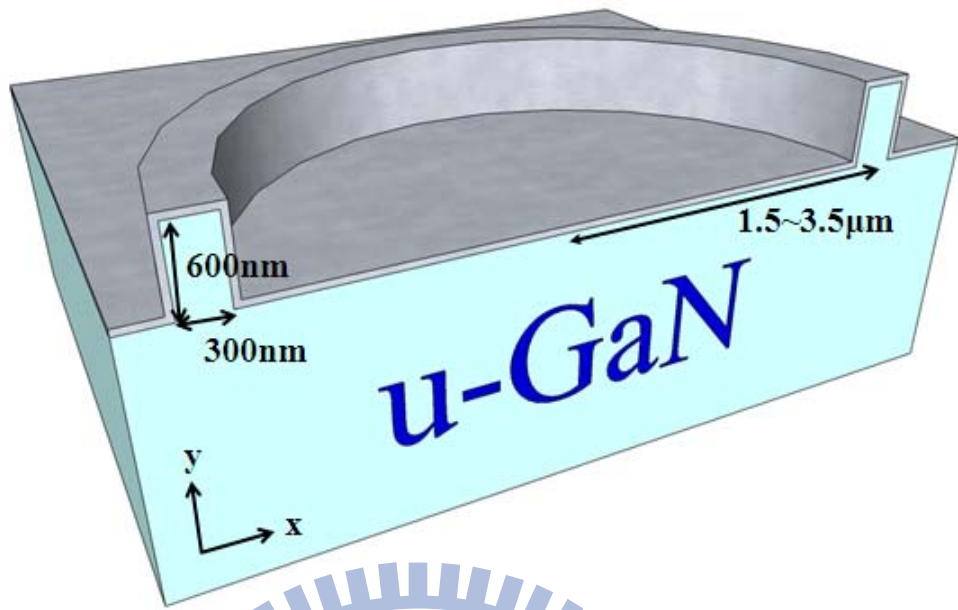


Fig. 4.1.4 Schematic Diagram of Metal-coated GaN Nanoring.



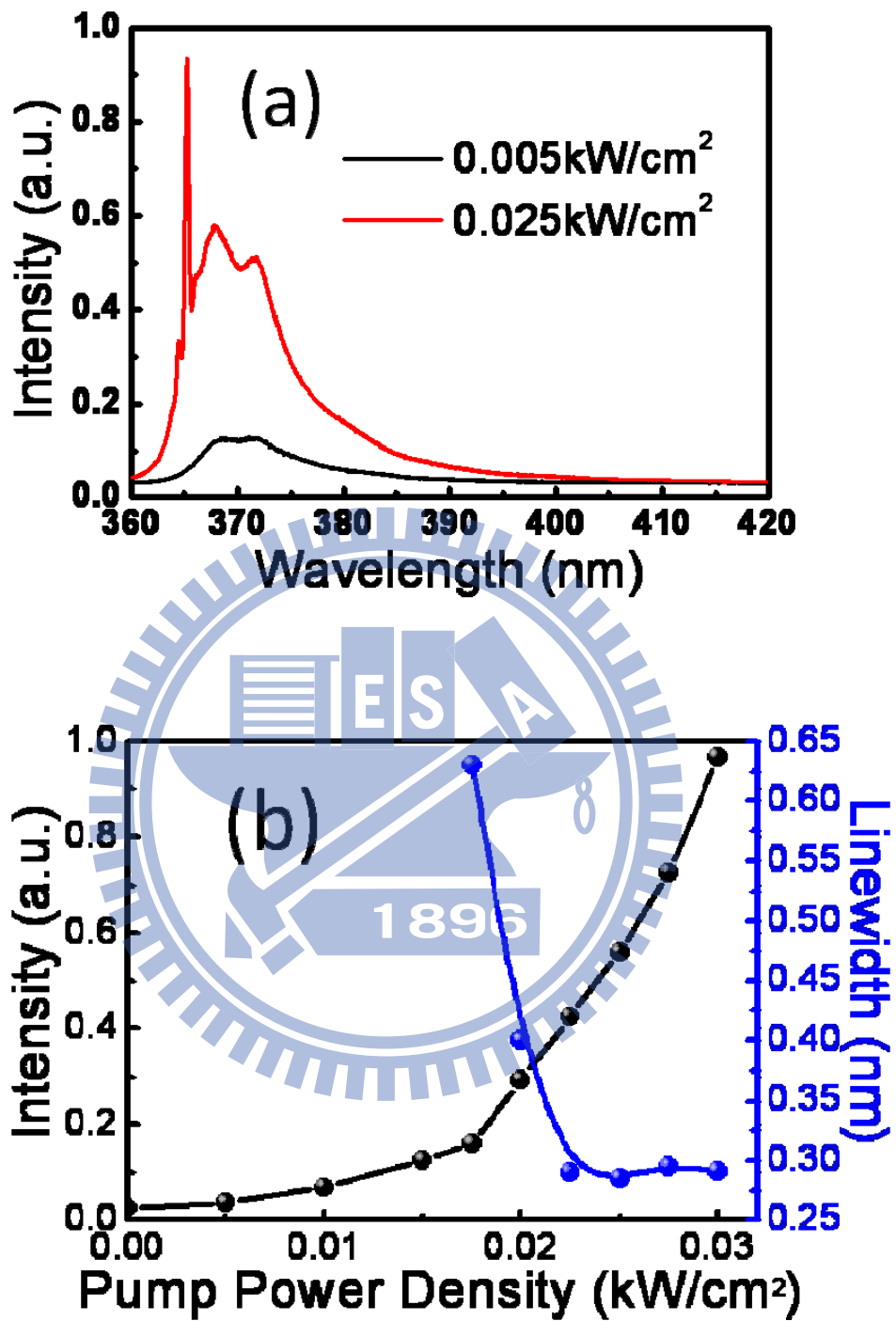


Fig. 4.2.1 Lasing Characteristics of Metal-coated GaN Nanoring with 7 μm in diameter (a) PL Spectrum Above (Red) and Below (black) Threshold. (b) L-L Curve and the Linewidth of the Lasing Peak.

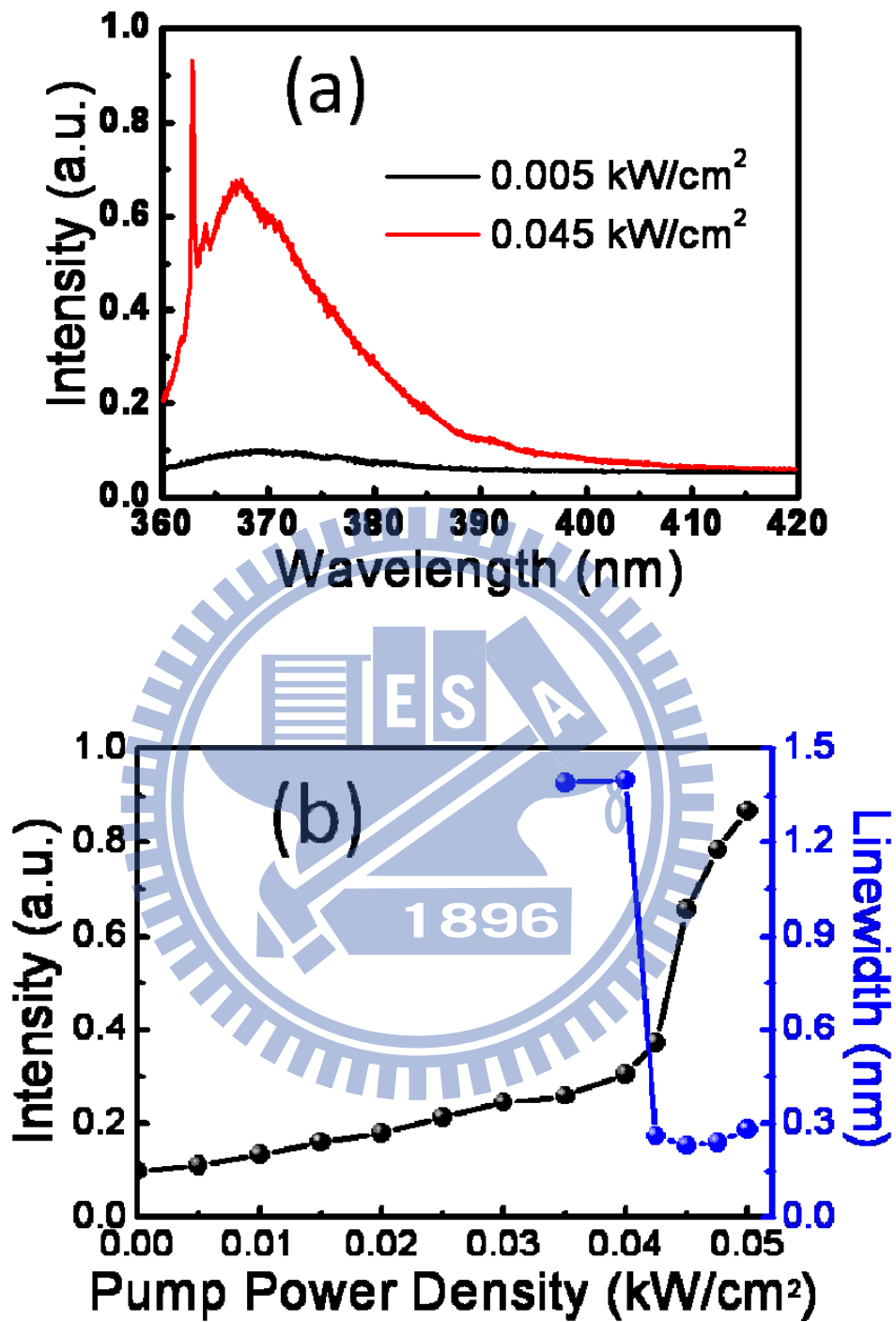


Fig. 4.2.2 Lasing Characteristics of Metal-coated GaN Nanoring with 5 μm in diameter (a) PL Spectrum Above (Red) and Below (black) Threshold. (b) L-L Curve and the Linewidth of the

Lasing Peak.

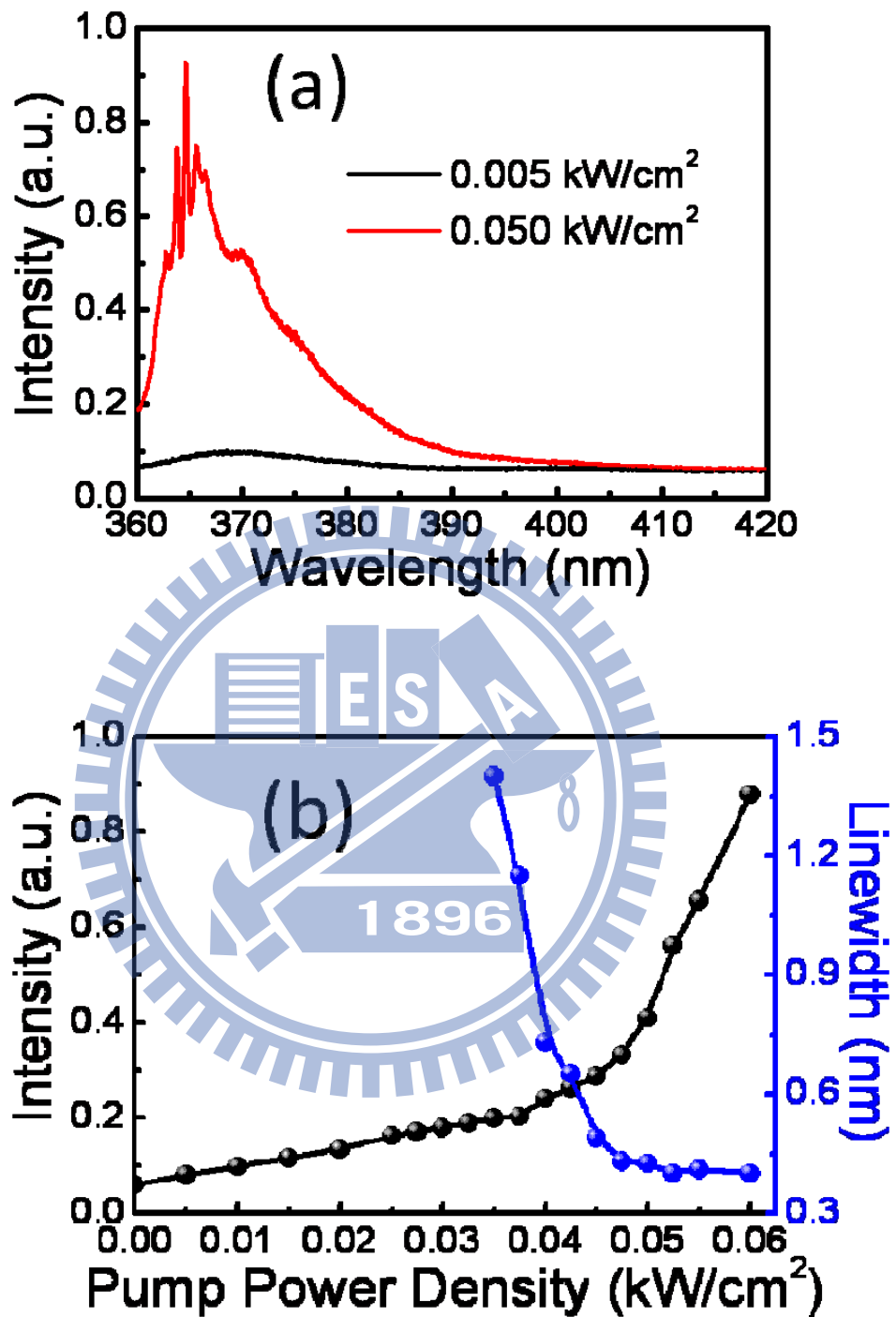


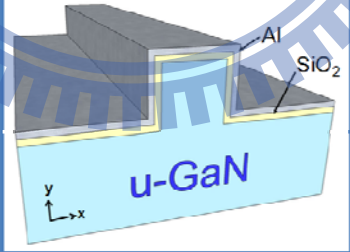
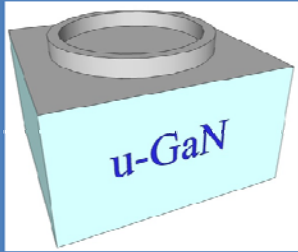
Fig. 4.2.3 Lasing Characteristics of Metal-coated GaN Nanoring with 3 μm in diameter (a) PL Spectrum Above (Red) and Below (black) Threshold. (b) L-L Curve and the Linewidth of the

Lasing Peak.

Table 4.2 Lasing Characteristics of Different Metal-coated GaN Nanorings.

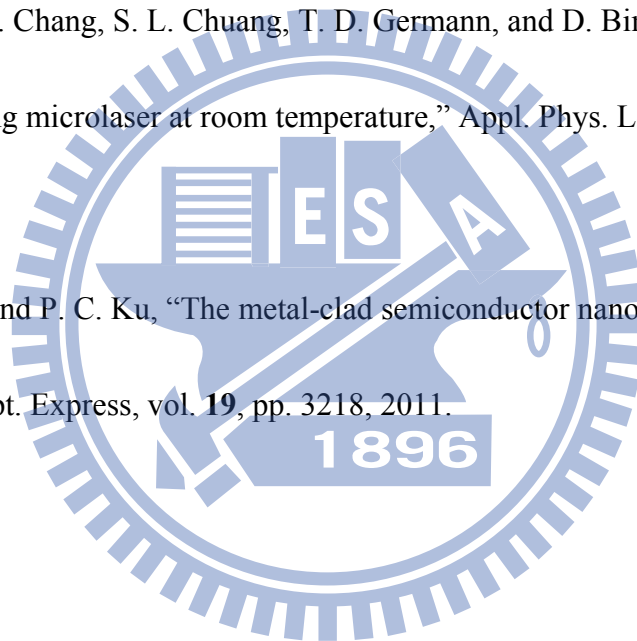
Geometrical Parameter of Nanoring (Height: 600nm)	Diameter: 7 μ m Width: 400nm	Diameter: 5 μ m Width: 340nm	Diameter: 3 μ m Width: 310nm
Lasing Wavelength (λ)	365nm	363nm	364nm
Quality Factor (Q)	~900	~900	~800
Threshold Power Density	0.019kW/cm ²	0.042kW/cm ²	0.045kW/cm ²
Compare to λ	Width: 1.09 λ	Width: 0.94 λ	Width: 0.85 λ

Table 4.3 Comparison between Metal-coated GaN Nanostripe and Nanoring.

Type of Metal-coated Nanocavity		
	Nanostripe	Nanoring
Size in μ m ³	12.5	1.7
Width of the Structure	1.35 λ (λ : 370nm)	0.85λ (λ : 364nm)
Quality Factor (Q)	~150	~800
Threshold Power Density	0.055kW/cm ²	0.045kW/cm²

References:

- [1] M. W. Kim, and P. C. Ku, "Lasing in metal-clad microring resonator," *Appl. Phys. Lett.*, vol. **98**, pp. 131107, 2011.
- [2] C. Y. Lu, S. W. Chang, S. H. Yang, and S. L. Chuang, "Quantum-dot laser with a metal-coated waveguide under continuous-wave operation at room temperature," *Appl. Phys. Lett.*, vol. **95**, pp. 233507, 2009.
- [3] C. Y. Lu, S. W. Chang, S. L. Chuang, T. D. Germann, and D. Bimberg, "Metal-cavity surface-emitting microlaser at room temperature," *Appl. Phys. Lett.*, vol. **96**, pp. 251101, 2010.
- [4] M. W. Kim, and P. C. Ku, "The metal-clad semiconductor nanoring laser and its scaling properties," *Opt. Express*, vol. **19**, pp. 3218, 2011.



Chapter 5 Conclusion

5.1 Conclusion

Lasing in metal-coated GaN nanocavity at room temperature is demonstrated. With the combination of GaN as gain medium and metal-coated nanocavity, lasing signal has been observed at room temperature in nanostripe and nanoring structure.

First, we observe a lasing peak with its wavelength is about 370nm and the quality factor is 150 for our metal-coated GaN nanostripe. It has a low threshold pump power density which is only 0.055kW/cm^2 (55mJ/cm^2). Moreover, by finite element method and effective index method, we prove that the aluminum layer coated on the nanostripe provides a better optical confinement and better thermal conductivity makes lasing action possible at room temperature and single mode lasing has been confirmed by the band diagram of the nanostripe structure and all these simulation results fit to experimental result pretty with only a small difference between them.

Second, we conduct fabrication process to make metal-coated GaN nanoring laser. The smallest ring we could observe lasing action at room temperature is $3\mu\text{m}$ in diameter, and the widths of the nanorings is about 310nm, smaller than the lasing wavelength. The quality factor of this device is about 800 and the threshold power density is only 0.045kW/cm^2 (45mJ/cm^2). Better performance and smaller device are obtained by the combination of nanoring structure and metal-coated nanocavity. The quality factor is improved and threshold

power density is smaller compare to metal-coated nanostripe. Also, better thermal stability of metal-coated device is confirmed by analyzing the PL spectrum of the devices. All these results shows promising way to further improve the device performance and shrink the size of device into subwavelength-scale.

5.2 Future Work

In order to achieve lasing in three-dimensional nanocavity or operate under electrically-pump condition, we have to reduce the optical loss in vertical direction. As shown in chapter 3, even though we could see clear standing wave pattern in the nanostripe structure, there is still some energy dissipate into the undoped GaN region beneath the structure. If we wanted to further improve device performance, we have to improve optical confinement vertically by heterostructure or Distributed Bragg reflector (DBR).

Moreover, poor injection efficiency of the measurement system might reduce the device performance. First, the beam spot size of Nd:YVO₄ laser is about 50 μ m, which is much larger than our device, lots of energy is wasted and might be the reason why there is always a signal around 370nm to 380nm in our spectrum. Smaller beam spot size comparable to the size of our device would significantly increase injection efficiency and the threshold power density might be smaller than what we get right now. Second, if we could use bonding technique to remove the sapphire substrate and undoped GaN layer beneath the device, we could collect lasing signal efficiently. It is hard for us to observe lasing signal because we are collect its

signal from top of the wafer, where is coated a high-reflectivity metal layer.

All the issues mentioned in the previous paragraphs are the key points for further development of metal-coated nanocavity. If we could solve these problems, we could achieve lasing in three dimensional or subwavelength nanocavity and photonic integrated circuit in nano-scale in the very near future.



Appendix

1. Thermal Issue

The thermal conductivity of metal is better than the air, therefore, it is believed that the device with metal layer coated on it would show a better performance after reduce the thermal effect. In our cases, the aluminum layer's thermal conductivity (237W/m-K) coated on the GaN nanocavities is far better than air (0.025W/m-K). We believe that this is also an important feature provided by metal so that we could observe lasing action at room temperature. From the lasing characteristics of GaN nanoring with and without metal, 5 μ m in diameter, we could observe the differences brought by metal layer.

From the PL spectrum, the lasing peak of the metal-coated nanolaser has a blue shift as the pumping power increase. However, for the GaN nanoring, 5 μ m in diameter, it has a red shift after a small blue shift as the pumping power increase, this indicates that the heat provided by pumping source influence the device performance. We believe that it is the metal layer coated on the nanoring structure passivates the heat provided by the pumping source, so that the device performance won't be affected by it. Fig. A. 1 shows the lasing peak wavelength of these two devices after turn on. This evidence shows that the metal layer coated on the nanocavity not only provide better optical confinement, but also better thermal dissipation that the device performance won't be influenced by heat even operate at high carrier density.

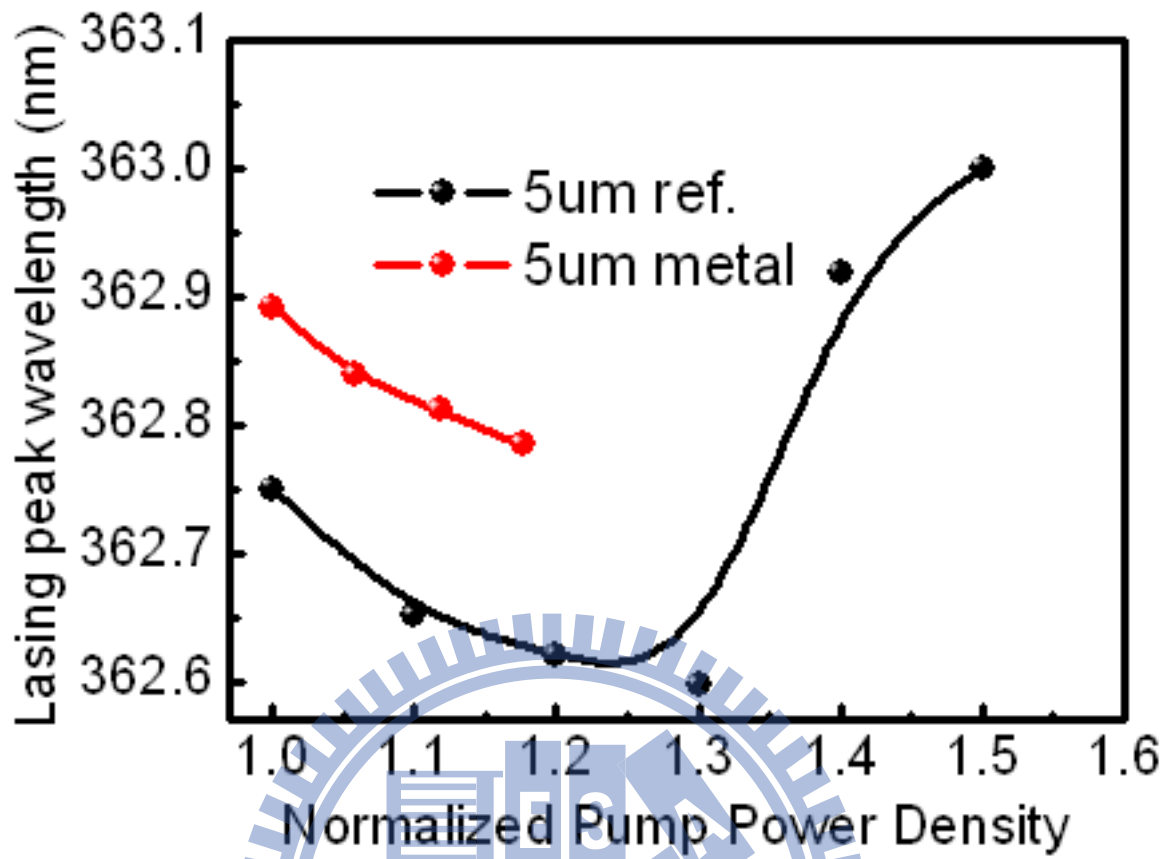


Fig. A.1 The Lasing Peak Wavelength of GaN Nanoring Laser with (Red) or without (Black) Metal.